Loss of age-associated increase in m^{6}A-modified RNA contributes to GABAergic dysregulation in Alzheimer's disease

Jenna L. Libera[1,2], Junming Hu[3¶], Tuyet-Anh Nguyen[1¶], Zihan Wang[1], Sophie J. F. van der Spek[1], Kamryn Schult[1], Luke Dorrian[1], Jordan Majka[4], Katarnut Tobunluepop[1], Sambhavi Puri[1], Alexander Kynshov[3], Nicholas M. Kanaan[5], Peter T. Nelson[6,7], Kate Meyer[8,9], Lei Hou[3], Xiaoling Zhang*[3,10,11], Benjamin Wolozin*[1,2,12]

[1]Department of Anatomy and Neurobiology, Boston University Chobanian and Avedisian School of Medicine, Boston, MA

[2]Department of Pharmacology, Physiology and Biophysics, Boston University Chobanian and Avedisian School of Medicine, Boston, MA

[3]Department of Medicine (Biomedical Genetics), Boston University Chobanian and Avedisian School of Medicine, Boston, MA

[4]Dyno Therapeutics, Watertown, MA

[5]Dept. of Translational Neuroscience, College of Human Medicine, Michigan State University, Grand Rapids, MI 49503.

[6]Department of Pathology and Laboratory Medicine and [7]Sanders-Brown Center on Aging, University of Kentucky, Lexington, KY

[8]Dept. of Biochemistry and [9]Dept. of Neurobiology, Duke University, Durham, NC

[10]Departments of Biostatistics, Boston University School of Public Health, Boston, MA

[11]Framingham Heart Study, Boston University Chobanian and Avedisian School of Medicine, Boston, MA

[12]Department of Neurology, Boston University Chobanian and Avedisian School of Medicine, Boston, MA

[¶]Co-equal contribution

*Corresponding Authors

Benjamin Wolozin, bwolozin@bu.edu

Xiaoling Zhang, xiaoling@bu.edu

HIGHLIGHTS

- With age, the number of m^6A sites increases among Control cases (lacking AD pathology) but remains unchanged in AD cases.
- Transcripts are globally hypomethylated in AD cases.
- Hypomethylation is linked to decreased mRNA expression of transcripts related to synaptic and proteostatic function in AD.
- 3'UTR-localized m^6A sites lack typical association with transcript metabolism of *GABRA1* in AD.

KEY WORDS

Alzheimer's disease | aging | N^6-methyladenosine (m^6A) | tripartite synapses | GABAergic signaling | proteostasis | RNA translation

ABSTRACT

Dysregulated RNA metabolism is a significant feature of Alzheimer's disease (AD), yet how post-transcriptional RNA modifications like N^6-methyladenosine (m^6A) are altered in AD is unknown. Here, we performed deamination adjacent to RNA modification targets (DART-seq) on human dorsolateral prefrontal cortices to assess changes in m^6A with nucleotide resolution. In non-AD brains, m^6A sites increased with age, predominantly within the 3′UTR of transcripts encoding tripartite synapse proteins. In contrast, AD brains lost the age-associated m^6A site increase and exhibited global hypomethylation of transcripts, including *MAPT* and *APP*. Hypomethylated genes involved with GABAergic signaling, glutamate transport, and ubiquitin-mediated proteolysis exhibited reduced expression, connecting m^6A to synaptic excitotoxicity and disrupted proteostasis in AD. Site-specific m^6A levels were linked with *GABRA1* expression and protein levels, but this relationship was abolished in AD. Our findings provide insight into post-transcriptional mechanisms of dysregulated RNA metabolism in AD that are related to aging and GABAergic regulation.

INTRODUCTION

Increasing evidence implicates RNA metabolic dysfunction in the pathophysiology of neurodegenerative diseases, including Alzheimer's disease (AD). For instance, disease-linked RNA binding proteins (RBPs), as well as the microtubule-associated protein tau (MAPT), have intrinsically disordered regions that are prone to aggregation in neurodegenerative diseases (King *et al*., 2012; Zhu *et al*., 2015; Maziuk *et al*., 2017; Dobra *et al*., 2018; Mittag & Parker, 2018; Ainani *et al*., 2023). This aggregation leads to a loss of functional soluble RBPs, causing dysfunction of RNA metabolism (Ross & Poirier, 2004; Wolozin & Apicco, 2014; Conti *et al*., 2016; Li & Sun, 2025). In amyotrophic lateral sclerosis (ALS), mislocalization and aggregation of TDP-43 in the cytoplasm enable cryptic splicing in the nucleus, resulting in production of proteins with deleterious structures (Ling *et al*., 2015; Hsieh *et al*., 2019; Apicco *et al*., 2019; Ma *et al*., 2022; Baughn *et al*., 2023). Other RBPs that mislocalize and aggregate in the cytoplasm also impact splicing and RNA stability, such as HNRNPA2B1, FUS, Ataxin-2, TIA-1 and Musashi (Kaehler *et al*., 2012; Wang *et al*., 2014; Martinez *et al*., 2016; Marrone *et al*., 2019; Liu & Shi, 2020; Montalbano *et al*., 2020; Silanes *et al*., 2023). We demonstrated that TIA-1 facilitates tau misfolding and aggregation in AD (Vanderweyde *et al*., 2016; Apicco *et al*., 2017; Jiang *et al*., 2018; Ash *et al*., 2021) However, the relationship between pathological tau and changes in RNA metabolism is poorly understood. Poly-serine-containing RBPs become sequestered with tau, promoting aberrant RNA splicing and exacerbating tau pathology (Lester *et al*., 2023). We reported that HNRNPA2B1 interacts with oligomeric tau in AD to regulate the translational stress response (Jiang *et al*., 2021a). Interestingly, HNRNPA2B1 primarily binds RNA that contains one of the most abundant RNA modifications, N^6-methyladenosine (m^6A; Alarcón *et al*., 2015; Wu *et al*., 2018; Liu & Shi, 2020, Jiang *et al*., 2021b). The role of HNRNPA2B1 as an m^6A-modified-RNA binding protein prompted transcriptional investigation of the m^6A landscape in AD that is now reported in this manuscript.

m^6A is a dynamic RNA modification installed by methyltransferases (i.e., writers) in the nucleus and removed by demethylases (i.e., erasers) in the nucleus and cytoplasm (Meyer & Jaffrey, 2017; Zhang, Qian, & Jia, 2021). These modifications occur in DRACH motifs (D = A/G/U, R = A/G, A = A or m^6A if methylated, C = C, and H = A/C/U), which are common sequences found in mRNA transcripts (Linder *et al*., 2015; Zaccara & Jaffrey, 2020). Studies

suggest that m^6A affects both nuclear and cytoplasmic processes of mRNA metabolism, including transcription, mRNA splicing, nucleocytoplasmic export, localization, translation, stability, and even stress granule formation (Anders *et al*., 2018; Ries *et al*., 2019; Fu & Zhuang, 2020; Murakami & Jaffrey, 2022; Sikorski *et al*., 2023). These functions are regulated by a wide range of "readers", or RBPs, that bind m^6A-modified RNA (Flamand, Tegowski, & Meyer, 2023; Zaccara & Jaffrey, 2024; Zou & He, 2024). TDP-43 and HNRNPA2B1 as just mentioned are both m^6A readers (Alarcón *et al*., 2015; McMillan *et al*., 2023); the dysregulation of another well characterized reader, FMRP, impairs synaptic development and translation and causes Fragile X-associated tremor/ataxia syndrome (Feng *et al*., 1997; Zhang *et al*., 2018 Edens *et al*., 2019; Hsu *et al*.., 2019; Richter & Zhao, 2024). The involvement of m^6A readers in neurodegenerative diseases connects m^6A-associated RNA metabolism with AD; however, the role of m^6A-modified transcripts in the AD brain is unknown.

Only recently is m^6A being investigated in the context of neurobiology and neurodegeneration. Emerging studies on the role of m^6A in the brain indicate that neurons uniquely leverage cytoplasmic m^6A for spatially regulated translation in the axon, dendrites, and synapses (Yu *et al*., 2018; Meyer, 2019; Tegowski & Meyer, 2024). This occurs on neuronal mRNAs, such as CAMKII and MAP2, and is regulated by 3'UTR-specific m^6A labeling (Flamand & Meyer, 2022; Castro-Hernández *et al*., 2023). The synaptic m^6A epitranscriptome promotes synthesis and modulation of tripartite synapses and is implicated in neurodevelopmental and neuropsychiatric diseases (Merkurjev *et al*., 2018). Almost every analysis of the human or mouse brain m^6A epitranscriptomes performed to date has relied on m^6A-antibody-based approaches by methylated RNA immunoprecipitation and sequencing (MeRIP-seq; Dominissini *et al*., 2012; Dominissini *et al*., 2013; Castro-Hernández *et al*., 2023). For instance, a recent MeRIP-seq study of C9ORF72-ALS/frontotemporal dementia observed decreased methylation and increased expression of many glutamatergic receptors and scaffolding genes, implicating synaptic excitotoxicity as a consequence of m^6A hypomethylation (Li *et al*., 2023). However, MeRIP lacks nucleotide-specific resolution and does not precisely quantify the m^6A level of genes (McIntyre *et al*., 2020). In addition, m^6A antibodies show cross-reactivity by binding the m^6Am RNA modification (Linder *et al*., 2015). To overcome these limitations, the Meyer group recently developed an m^6A sequencing method, termed "deamination adjacent to RNA modification targets" (DART-seq; Meyer, 2019). This method uses a fusion protein

consisting of the m^6A-binding YTH domain tethered to the C-to-U deaminase APOBEC1 to achieve targeted editing of cytidines that follow m^6A sites (Linder *et al*., 2015). Importantly, this method characterizes m^6A at the single nucleotide level across the transcriptome, which we leveraged to identify changes in m^6A sites and m^6A level that occur in human AD brains.

Using DART-seq profiles from the dorsolateral prefrontal cortex, we now report the first single-nucleotide characterization of m^6A differences between human post-mortem AD and non-AD Control cases (n=19/cohort). We observe a striking age-dependent increase in m^6A-modified sites in Control cases, evident globally as well as in genes regulating the tripartite synapse; methylation of genes related to GABAergic signaling and glutamate transport coordinate with their mRNA expression. In contrast, AD cases lack this age-dependent increase of m^6A-modified sites, suggesting that m^6A modifications in AD are driven by the disease process rather than by aging (across 70-, 80-, and 90-year-old cases). AD cases show global hypomethylation of genes, including disease-linked genes like amyloid precursor protein (*APP*) and *MAPT*, and those related to ubiquitin-mediated proteolysis. Tripartite synapse genes *GABRA1*, *GABRA2*, *GABRA4*, and *SLC1A2* also exhibit hypomethylated 3'UTR*s* and reduced expression in AD, implicating excitotoxicity. Methylation level of specific sites in the 3'UTR of *GABRA1* is linked with mRNA and protein level of *GABRA1* in Control cases, but this relationship is lost in AD cases, possibly reflecting disease-related dysfunction. These results reveal a strong role for m^6A in the aging process and in the response of synaptic dysfunction to the disease process.

RESULTS

Validation of DART-seq confirms detection of m^6A sites in human post-mortem brains.

Detection of m^6A sites at the single-nucleotide level was accomplished by performing DART-seq on RNA from human post-mortem brains (**Table 1**). We analyzed age-matched (**Fig. S1A**) and sex-matched (**Fig. S1B**) neurologically normal Control and AD brains (n=19 each). As per the diagnostic criteria, AD cases had higher tau burden (**Fig. S1C**) and amyloid burden (**Fig. S1D**) than Control cases. The majority of AD cases were *APOE ε3/ε4* carriers while most Control cases were *APOE ε3/ε3* carriers (**Fig. S1E**). Notably, in both cohorts, brain samples were collected with a mean post-mortem interval of ~2.5 hours (**Fig. S1F**); the RNA quality for each sample was >7 RIN^e pre-DART reaction and >6 RIN^e post-DART reaction (**Fig. S1G**), highlighting robust sample quality.

To ensure feasibility of the DART-seq method on our human post-mortem brains, we standardized a workflow involving automated sample homogenization, multiple rounds of RNA purification, and quality control checks of RNA and cDNA libraries using a Tapestation 4200 (Agilent). (**Fig. S2A**). Two m^6A sites along the *ACTB* transcript, A1222 and A1248, were previously reported to have high levels of m^6A (Tegowski, Zhu, & Meyer, 2022). We validated m^6A level of these sites in a subset of the samples (n=3/cohort) by incubating RNA in parallel conditions with APOBEC1-YTH to induce C>U editing and with APOBEC1-YTH^{mut} as a negative control, performing PCR to amplify the sites, and quantifying the proportion of C>U editing as given by Sanger sequencing. DART-seq on our full sample set used next generation sequencing and the Bullseye pipeline to uncover novel m^6A sites (Flamand & Meyer, 2022; Tegowski, Flamand, & Meyer, 2022; Zhu *et al*., 2022; Tegowski *et al*., 2024; **Fig. 1A**). Indeed, our C>U editing was ~16% at A1222 and ~32% at A1248 of RNA incubated with APOBEC1-YTH (**Fig. S2B**); RNA that was incubated with APOBEC1-YTH^{mut} was edited ~50% less (**Fig. S2C**). These levels match prior reports (Tegowski, Zhu, & Meyer, 2022; Tegowski & Meyer, 2022). We also profiled C>U conversion of A1035, a non-methylated DRACH motif, and observed almost no editing (~1-5%, **Fig. S2B**). This confirms that DART is specific to m^6A-occupied DRACH motifs as previously reported (Meyer, 2019; Tegowski, Flamand, & Meyer; 2022). Importantly, DART-seq identified sites A1222 and A1248 across all 38 samples, showing

similar C>U conversion to our PCR validation (**Fig. S2D**). Together, these results demonstrate validity of DART-seq on human post-mortem brains.

Loss of age-dependent m^6A sites on genes involved in synaptic function occurs in Alzheimer's disease.

DART-seq of all 38 brains revealed 36,596 m^6A sites across 6,878 genes (**Fig. 1B, Table 2**). The distribution of m^6A sites across the mRNA transcript showed that sites were most abundant in the CDS (**Fig. 1C**), matching distribution curves from prior DART-seq studies (Flamand & Meyer, 2022; McMillan *et al*., 2023). These sites were significantly enriched for the DRACH motif (*P*=1.0e-331, **Fig. S3A**). A KEGG pathway analysis included RNA metabolism (e.g., "mRNA surveillance pathway", "Spliceosome", "Nucleocytoplasmic transport") among the top 5 enriched groups of genes with m^6A sites, followed by many neurodegenerative terms including "Alzheimer disease" (**Fig. 1D**). A trending decrease in the number of total m^6A sites was observed in AD cases compared to Control cases (**Fig. 1E**). There were also trending decreases in the number of 5'UTR, CDS, 3'UTR, and ncRNA m^6A sites for AD cases compared to Control cases (**Fig. S4A-D**). However, total number of m^6A sites demonstrated a significant correlation when compared against age as an endophenotype (**Table 1; Fig. 1F**). Increasing age (beginning at age 70 years) associated with increased m^6A sites of specific mRNA domains, including the 5'UTR, CDS, and 3'UTR, but not on ncRNA (**Fig. 1G, Fig. S4E-H**). Interestingly, the correlation of age with m^6A sites was seen only in the Control cases; AD cases exhibited no correlation of age with the amount of m^6A sites. The stable number of m^6A sites in AD across age suggests that the disease process is the primary factor driving m^6A site occurrence in AD (**Fig. S3B**). The age-dependent increase in m^6A sites was seen most strongly in the 3'UTR among Control cases but was also present in the 5'UTR, CDS, and ncRNAs (**Fig. 1H, Fig.S4I-K**). To better understand the role of m^6A in the 3'UTR, we performed a KEGG pathway analysis on genes with 3'UTR-containing m^6A sites across all cases, which revealed "GABAergic synapse" as the most highly enriched term (**Fig. 1I**). Gene ontology (GO) Cell Compartment (CC) analyses strengthened the link of m^6A to synaptic biology, showing "Glutamatergic synapse" as the most highly enriched term among genes with 3'UTR-localized m^6A sites (**Fig. S5D**). Synaptic terms were also among the most enriched in all m^6A-containing genes and gene locations (except the CDS) (**Fig. S5A-E**). These data suggest that increasing m^6A-modified sites

is a feature of neurologically normal aging, which fails to occur in AD. The most vulnerable sites and associated pathways affected by the disease occur at 3'UTR sites involved in GABAergic functioning and glutamatergic synapses.

Differentially abundant m^6A sites converge on tau phosphorylation, RNA metabolism, and GABA-A receptors.

Next, we looked at whether there were differential m^6A sites between Control and AD cases that could be related to disease mechanisms and synaptic function. To achieve this, we analyzed the number of Control and AD cases at each specific m^6A site and determined whether that site was overrepresented among Control or AD cases (i.e., differentially abundant sites, DAS, **Table 3**). Sites were differentially abundant in Control cases if >50% of cases had a site and <10% of AD cases had a site. Conversely, DAS in AD cases had >50% representation and <10% representation in Control cases. Control cases displayed 328 DAS across 209 genes while AD cases had only 137 DAS across 131 genes (**Fig. S6A-B**). The proportion of DAS identified between Control and AD cases was similar among all gene domains. (**Fig. S6C**). Among the most relevant DAS were those found in genes involved with tau phosphorylation status (e.g., *FYN*, *PPP1CB*, *PPP2R5C*) tau misfolding (e.g., *HSP90* paralogs), stress surveillance (e.g., *EIF2AK2/PKR*, *HIF1A*) stress granules (e.g., *TAF15*, *HNRNPC*, *DDX5*, *CAPRIN1*, *G3BP1*), and glutamatergic/GABAergic receptors (e.g., *GRIN2A*, *GRIN2B*, *GABRA* paralogs) (**Fig. S6D**). In particular, the DAS on *FYN*, *HSP90AA1*, and *TAF15* were found uniquely in AD cases and were completely absent in Control cases (**Fig. S6E**), suggesting that these may be key m^6A sites that mediate pathological processes among AD cases specifically. The link between DAS and disease was also evident with a GO CC analysis, for which the most enriched terms for DAS in AD cases included phosphatase complexes (**Fig. S6G**). In contrast, DAS in Control cases showed the most enrichment among GABAergic processes, such as "Benzodiazepine receptor activity", by GO Molecular Function (**Fig. S6F**). Together, these data suggest that there are cohort-exclusive m^6A sites that have unique, different functions in the normal brain (i.e., in Control cases, regulating GABAergic signaling) and the diseased brain (i.e., in AD cases, regulating tau phosphatases).

Hypomethylation of m^6A-modified transcripts in Alzheimer's disease includes *MAPT* and *APP* and is associated with altered mRNA expression and protein levels.

We next quantified the mean level of m^6A methylation of genes or gene domains for each cohort, characterizing differential methylation between AD and Control cases at the gene-level and gene domain-level (as previously described in Flamand & Meyer, 2022; **Table 4**). Strikingly, almost all DMGs were hypomethylated in AD (**Fig. 2A**), while RNA-seq revealed an equal number of upregulated and downregulated differentially expressed genes (DEGs, **Fig. 2B, Table 5-6**). The RNA-seq is consistent with prior datasets, such as from the Mount Sinai Brain Bank (MSBB, https://adknowledgeportal.org/, **Fig. 2B-C**). The global reduction of m^6A level among AD cases occurs independently of transcript level (**Fig. 2D**); little overlap was also observed between differentially methylated domains (i.e., mean levels of methylation that include all the m^6A sites within specific regions of the gene corresponding to the 5'UTR, CDS, 3'UTR, or ncRNAs) and DEGs (**Fig. S7A-H, *see Table 4*)**. The hypomethylated DMGs included *MAPT* and *APP*, which are methylated exclusively in the 3'UTR and do not show differential mRNA expression (**Fig. 2E, *see Table 6***). To check for protein levels, we purified brain lysate from our Control and AD cases and quantified levels of MAPT and APP by immunoblot. In AD cases, there was a 1.9x increase in MAPT and a 1.5x increase in APP compared to Control cases (**Fig. 2F-2I**). These findings raise the possibility of m^6A-mediated regulation of protein synthesis, as this has been demonstrated before in cultured human and mouse neurons (Weng *et al*., 2018; Flamand & Meyer, 2022; Castro-Hernández *et al*., 2023). We proceeded to explore the interaction between m^6A and MAPT and APP protein levels by examining AD endophenotypes. Both MAPT and APP protein levels positively associated with tau burden (i.e., Braak stage) and amyloid burden (i.e., Thal phase, **Fig. 2J-K**). MAPT protein level showed a trending negative association with *MAPT* m^6A level whereas APP protein level showed a significant negative association with *APP* mRNA level. However, *APP* mRNA level positively associated with *APP* m^6A level, which negatively associated with Braak stage. These data reflect the possibility of m^6A-mediated translation of MAPT and APP tanscripts. DART-seq revealed two methylated DRACH sites at positions A4375 and A5942 of *MAPT* (**Fig. 2E, *see Table 2***); the m^6A level at site A5942 was negatively associated with Braak stage. For *APP*, we uncovered three methylated DRACH sites at positions A3365, A3358, and A2987 (**Fig. 2E, *see Table 2***); the m^6A level at site A3365 was positively correlated with APP protein level, although the total m^6A level of *APP* transcript did not correlate with protein level. Interestingly, none of the individual m^6A site levels of *APP* associated with *APP* mRNA level, despite total m^6A level of *APP* positively

correlating with *APP* mRNA level. These findings highlight differences of m^6A regulation at the site-level and gene-level and reveal that m^6A methylation of *MAPT* and *APP* associates differentially between their mRNA and protein levels. These data also demonstrate that m^6A methylation for *MAPT* and *APP* shows a stronger correlation with tau burden than with amyloid burden.

GABAergic synapses and proteolysis show strong gene set enrichment for m^6A-linked expression.

The strong DAS signature for GABAergic transcripts is also present among enriched gene sets that are shared between DART-seq (m^6A) and RNA-seq (transcription) datasets. Gene set enrichment analysis (GSEA) of the DART-seq dataset revealed that most enriched groups include many synaptic terms (e.g., "Synaptic vesicle cycle", "GABAergic synapse", and "Glutamatergic synapse"); other enriched groups include protein-related terms (e.g., "Ubiquitin mediated proteolysis", "Protein processing in the endoplasmic reticulum", and "Motor proteins"; **Fig. 3A, Table 7**). Synaptic terms (e.g., "Synaptic vesicle cycle" and "GABAergic synapse") are also enriched in the RNA-seq dataset with many more neurodegenerative terms included (e.g., "Parkinson disease", "Prion disease", and "Alzheimer disease", **Fig. 3B, Table 8**). Other terms enriched in the RNA-seq dataset are related to proteostasis (e.g., "Ribosome", "Proteasome", and "Ubiquitin mediated proteolysis"). Four enriched gene sets overlapped between DART-seq and RNA-seq: "GABAergic synapse", "Nicotine addiction", "Synaptic vesicle cycle", and "Ubiquitin mediated proteolysis" (**Fig. 3C**). This suggests that these gene sets in particular have a strong link between m^6A level and mRNA level. The GABAergic synapse gene set includes multiple elements beyond the obvious signature of GABAergic receptors, including *SLC38A1* (i.e., *SNAT1*, a glutamine transporter) and *GLUL* (i.e., glutamine synthetase that removes glutamate by conversion to glutamine). The glutamate transporter *SLC1A2* (i.e., *EAAT2* or *GLT-1*) was also included in "Synaptic vesicle cycle", linking potential impairment in glutamate uptake from synapses with excitotoxicity in AD. Other terms enriched in "Synaptic vesicle cycle" are *ATP6V* genes, *SNAP25*, and *CLTC* indicating the potential dysfunction of synaptic vesicle acidification, exocytosis, and endocytosis in AD (**Fig. 3F**). Neddylation and ubiquitination are also important elements of synaptic function (although not restricted to synaptic function) and correspondingly the term "Ubiquitin mediated proteolysis" showed enrichment for genes including *UBA*, *UBE*,

and *CUL* paralogs (**Fig. 3G**). Together, these data suggest that in AD, hypomethylated genes contribute to aberrant functioning of GABAergic signaling, synaptic vesicle cycling, and ubiquitin-mediated proteolysis by associating with reduced mRNA expression.

Alzheimer's disease brains lack an age-related, m^{6}A increase of tripartite synapse genes.

We next determined which genes are shared among the enriched synaptic gene sets from DART-seq to identify synaptic targets linked to m^{6}A-mediated synaptic impairment in AD. Our network plot revealed a striking coalescence of genes linked to the tripartite synapse, including GABAergic receptors (*GABRA1*, *GABRA2*, *GABRA4*), glutamatergic receptors (*GRIA1*, *GRIA2*, *GRIA3*, *GRIN2A*, *GRIN2B*) and glutamate/glutamine interacting proteins (*SLC1A2/EAAT2*, *SLC1A3*, *SLC38A1*, *GLUL*), as well as signaling molecules regulating this axis (kinases, phosphatases, calcium binding proteins, **Fig. 4A, yellow circles**).

The strong increase in m^{6}A sites observed with aging in Control cases prompted us to examine this phenomenon among the tripartite synapse genes. First, we uncovered several genes in the pre-synapse, astrocyte, and post-synapse that are hypomethylated in AD (**Fig. 4B-E**). Then, we identified genes with differential 3'UTR-m^{6}A level, given that we found the strongest age-related m^{6}A effect among 3'UTR sites (**Fig. 1H, 4F**). GABAergic receptors, notably *GABRA1*, and *SLC38A1* showed striking age-related increases in m^{6}A methylation, but only in Control cases (**Fig. 4G-H, S8A-F**). In contrast, AD cases showed no change in m^{6}A levels with age, suggesting a disease effect and lack of age-linked adaptation.

We proceeded to examine how the increase in m^{6}A methylation impacts tripartite synapse gene expression. Expression of tripartite synapse genes is largely reduced in AD (**Fig. S9A, *see Table 5***). Linear regressions among all cases demonstrated a strong link between m^{6}A methylation and transcript expression for the GABAergic genes and glutamate/glutamine transporters *SLC1A2* and *SLC38A1*, but not for *GLUL* (**Fig. 4I-K, S9B-D**); increased m^{6}A methylation correlated significantly with increased transcript expression. The specific transcriptional patterns of m^{6}A regulation are notable for occurring among transcripts that would mitigate increased glutamatergic signaling, potentially providing synaptic resilience in cognitively normal individuals. In contrast, deleterious glutamatergic signaling is a well-known feature of the pathophysiology of AD (Hynd, Scott, & Dodd, 2004; Rudy *et al*., 2015), which is

potentially reflected by the absence of age-linked 3'UTR-m^6A regulation in mitigating the reduction of GABAergic and glutamate-transporting genes among AD cases.

Insufficient methylation of *GABRA1* in Alzheimer's disease abolishes the association of m^6A to GABRA1 fate.

Our strongest differential, age-related change in m^6A level was found on *GABRA1*, which was only one of twenty-two genes that exhibited transcriptome-wide significant decreases in expression and methylation in AD (**Fig. S9E, *see Table 4 and Table 6***). To explore this relationship, we performed DART-PCR followed by Sanger sequencing, qPCR, and immunoblot experiments to link methylation, expression, and protein level with aging. There are 7 3'UTR m^6A sites on *GABRA1* that were identified by our initial transcriptome-wide DART-seq approach, which showed variable levels of hypomethylation in AD by targeted DART-PCR and Sanger sequencing (**Fig. 5A, *see Table 2***). These sites also had variable degrees of C>U editing that were specific to cytidines only in DRACH motifs (**Fig. 5B**). After summing the m^6A levels of these sites, we confirmed the age-dependent increase of 3'UTR m^6A level of *GABRA1* in Control cases, which was lost in AD cases (**Fig. 5C**). qPCR of total *GABRA1* level also matched our previous RNA-seq results showing 50% downregulation in AD cases compared to Control cases (**Fig. 5D**, ***see Table 6***); however, we did not observe an effect of age at the transcript level here (**Fig. 5E**). We performed synaptosome isolation on our Control and AD cases (**Fig. 5F, Table 9**) and confirmed enrichment of GABRA1 protein in the synaptosomal fraction over the whole homogenate fraction (**Fig. 5G**). We quantified a significant decrease in synaptosomal GABRA1 protein in AD cases compared to Control cases (**Fig. 5H**); no effect of age on synaptic GABRA1 protein level was apparent (**Fig. 5I**).

We then generated correlation matrices to understand how the relationship between GABRA1 metabolism and age may be different for Control cases compared to AD cases. In Control cases, the 3'UTR m^6A level of *GABRA1* positively associated with age, and m^6A levels of various 3'UTR DRACH sites associated with *GABRA1* expression, protein level in the homogenate, and protein level in the synaptosome (**Fig. 6A**). Conversely in AD cases, total 3'UTR m^6A level of *GABRA1* had no association with age, although individual 3'UTR DRACH sites did show an age-related correlation (**Fig. 6B**). Remarkably, the relationship of individually methylated *GABRA1* 3'UTR DRACH sites with expression or protein level of GABRA1 was

also abolished. These associations suggest that a critical level of m^6A may exist to elicit control over transcript metabolism, which in AD, could be too low to be met for *GABRA1* (**Fig. 6C**).

DISCUSSION

RNA modifications, such as m^6A methylation, represent a key level of control for RNA metabolism and are only recently being explored in neuroscience and neurodegenerative diseases. We present the first site-specific analysis of m^6A changes in the human AD brain and characterize m^6A changes at the site, domain, and gene levels. We uncovered over 36,500 sites across 6,800 genes that were enriched for transcripts regulating synaptic activity (**Fig. 1D**). Brain samples from cognitively normal individuals exhibit a strong increase in m^6A sites with age, which was seen most strongly in 3'UTR-localized m^6A sites (**Fig. 1H**). AD brains show a stable number of m^6A sites while having reduced levels of m^6A-modifications in transcripts (**Figs. 1E, 2A**). For instance, *MAPT* and *APP* transcripts exhibit hypomethylation in AD cases (**Fig. 2A**). The increase in m^6A labeling with age is particularly apparent in the GABAergic/glutamatergic tripartite synapse, where m^6A labeling correlates with expression level for GABA-A receptor α subunits *GABRA1*, *GABRA2*, and *GABRA4*, glutamate transporter *SLC1A2* (*EAAT2*), and glutamine transporter SLC38A1 (*SNAT1*, **Fig. 4I-K, S9B-C**). The absence of age-related adaptation of m^6A methylation suggests that the pathophysiology of AD disrupts the regulation of RNA metabolism through impaired m^6A methylation.

Aberrant m^6A methylation in AD appears to associate with dysregulation of the tripartite synapse axis. Disease-linked changes in m^6A sites occur on *GRIN2A*, *GRIN2B*, *GABRA1*, *GABRA2*, and *GABRA4* transcripts (**Fig. S6D**). This implicates disrupted neurotransmission by differential methylation of excitatory and inhibitory receptors at the site level. At the transcript level, *GABRA1*, *GABRA2*, *GABRA4*, *SLC1A2*, and *SLC38A1* all showed strong disease-linked hypomethylation in AD (**Figs. 4B-D**) and robust positive correlation between m^6A labeling and transcript levels (**Figs. 4I-K, S9B-C**). Correlation was also apparent between GABRA1 protein and m^6A level at particular *GABRA1* m^6A sites (**Fig. 6A**), which suggests that m^6A labeling, transcription and translation of the tripartite synaptic genes in AD are interconnected. Reduction in methylation of tripartite GABA receptors and glutamate transporters might contribute to the

detrimental excitatory signaling that occurs in many models of AD and is thought to occur in the brains of AD subjects (Masliah *et al*., 1996; Limon, Reyes-Ruiz, & Miledi, 2012; Takahashi *et al*., 2015; Carello-Collar *et al*., 2023). In contrast, cognitively normal Control brains exhibit progressive age-linked increases (across 70-, 80-, and 90-year-old cases) in m^6A levels in the 3'UTR, as seen for *GABRA1*, *GABRA2*, *GABRA4*, *SLC1A2*, and *SLC38A1* transcripts (**Figs. 4G-H, S8A-C, S8E**). This implicates m^6A in regulating GABAergic and glutamatergic signaling (**Figs. 1I, S5D**, **3A**, **4A**). Other studies noted increases in m^6A with aging but have not previously identified the role of the tripartite synaptic genes with aging (Shafik *et al*., 2021; Sun *et al*., 2022; Fan *et al*., 2023; Wu *et al*., 2023). Increased excitotoxic activity tends to occur with aging and disease (Brewer *et al*., 2007; Dong, Wang, & Qin, 2009; Baltan, 2014). The age-related increase in m^6A labeling of GABA receptors and glutamate transporters might reflect a protective compensatory response dampening excitatory activity, which is dysregulated in AD.

The general dysregulation of m^6A sites in the 3'UTR among AD cases suggests a widespread impairment of RNA metabolism, although it is important to note the CDS also contains many m^6A sites (**Fig. 1B**). In the brain, m^6A has been shown to influence transcript localization to synapses (Livneh *et al*., 2019; Widago & Anggono, 2018; Flamand & Meyer, 2019; Li *et al*., 2019; Zhang *et al*., 2022; Xia *et al*., 2023). The 3'UTR contains binding motifs that m^6A readers and RBPs can use to direct transcript localization to and translation at synapses (Karapetyan *et al*., 2013; Mayr, 2017). In AD, 3*'UTR*-directed hypomethylation of transcripts encoding tripartite synapse genes (**Fig. 4F**) could reflect a reduction in synaptic trafficking of transcripts, reducing the pool of available transcripts necessary for activity-dependent translation, neuroplasticity, and protection from excitotoxicity.

Tauopathies, including AD, elicit dysfunction of proteostasis with a concomitant stress response, which was reflected in the m^6A-transcriptome. Methylation of multiple related stress response transcripts was dysregulated in AD, including the translation regulators *EIF2AK2* (*PKR*), *EIF1AX*, *EIF4B*, and *EIF4BP3* (**Figs. 2A, S7D, S7, S9E**). The DAS for *EIF2AK2* (*PKR*) shows more consistent hypermethylation among AD cases than Control cases (**Fig. S6D**). This is striking given that more sites and genes are hypomethylated than hypermethylated in AD (**Fig. S6C, 2A**), suggesting an increase in stress-dependent regulation of translation in AD. Previous studies support the idea that m^6A is highly responsive to neuronal conditions; for instance, many

studies show that RNA translation decreases with stress and disease (Wolozin & Ivanov, 2019), and activity-dependent translation of m^6A-modified transcripts is also well-documented in the brain (Flamand & Meyer, 2022; Castro-Hernándeza *et al*., 2023, Shi *et al*., 2018; Zou *et al*., 2023). We also observed DAS for multiple *HSP90* paralogs, which might reflect impairment of proteostasis in AD with a resulting exacerbation of pathologies. Genes that regulate ubiquitin-mediated proteolysis, including ubiquitin conjugating enzyme genes (*UBE2D3*, *UBE2K*, *UBE2G1*) and Cullin family genes (*CUL4B*, *CUL5*, *CUL2*) are enriched in both the DART-seq and RNA-seq analyses (**Figs. 3A-C, 3G**). Thus, m^6A-linked downregulation of these genes might be associated with dysfunction of ubiquitin signaling and proteostasis, reducing protein clearance and potentially enhancing protein aggregation.

Many genes associated with AD pathophysiology showed differential m^6A levels. For example, *MAPT* is hypomethylated (**Fig. 2A**) and the m^6A level at DRACH site A5942 of *MAPT* negatively correlates with MAPT protein level. This suggests that in AD, reduction of m^6A on *MAPT* is linked with increased tau protein. Genes such as *FYN* (a kinase that phosphorylates tau at synapses; Lee *et al*., 2004; Meur & Karati, 2025) and *PPP1CB* (part of a tau phosphatase complex; Martin *et al*., 2013) have DAS in AD cases (**Fig. S6D**), linking m^6A to tau phosphorylation status. Interestingly, the DAS on *FYN* (chromosome position 111780572, **Table 3**) is a common SNP (rs12910, 0.47; NCBI dbSNP) that is associated with increased risk of alcohol dependence (Pastor *et al*., 2009); however, analysis of this SNP in AD databases (e.g., ADSP) fails to show any disease linkage. The methylation profile of *APP* behaves differently in comparison to that of *MAPT*. Hypomethylation of *APP* was reported in the aging mouse cortex using scDART-seq (Tegowski *et al*., 2024). Although we did not observe an age-association in the human brain, we confirmed that the *APP* gene is hypomethylated in AD, associating with an increase in Braak stage (i.e., tau burden, **Fig. 2K**). Other genes that are associated with AD pathophysiology and showed differential m^6A sites include the proteostasis genes *HSP90AA1*, *HSP90B1*, *HSP90AB1*, *HIF1A*, and the translational stress response genes *EIF2AK2*, *G3BP1*, *DDX5*, *HNRNPC* and *CAPRIN1; G3BP1* and *CAPRIN1* are essential for formation of stress granules (Reineke *et al*., 2015; Protter & Parker; 2016; Wolozin & Ivanov, 2019). These findings link aberrant m^6A methylation at the site and gene levels to well established players involved in AD pathophysiology. Restoring methylation of these sites to non-AD levels could offer an alternative mechanism of AD intervention.

The studies reported in this manuscript provide a benchmark for understanding how m^6A methylation responds to aging and neurodegeneration in humans. The nucleotide level analysis for the human m^6A epitranscriptome provides an important reference for interpreting other studies using less precise approaches, such as MeRIP-seq and/or studies that use animal models that incompletely reflect AD pathophysiology. The reduced precision of MeRIP-seq combined with differences between the human condition and animal models might contribute to variable results among m^6A studies in the literature. A small study of human brain samples (n=6, using MeRIP-seq) shows similar results with increased m^6A methylation of mRNA in the normal aged human brain region Brodmann Area 10 (Castro-Hernández *et al*., 2023). Studies of aging in Drosophila also indicate that m^6A increases with age in the brain (Perlegos, Byrns, & Bonini, 2024). Mixed results of m^6A in aging were observed among studies using mouse models of AD that express human APP/PS1 or human APP (mut) knock-in/P301S Tau (Han *et al*., 2020; Zhao *et al*., 2021; Jiang *et al*., 2024) and Drosophila models expressing human R406W tau (Atrian *et al*., 2024). Total m^6A appears to increase, but m^6A methylation of specific mRNA transcripts tends to be lower. Our prior work also demonstrated an m^6A increase with disease severity among neurons showing AD pathology (Jiang *et al*., 2021). However, the results from our prior work relied on antibody-based imaging and ELISA experiments, which do not discriminate between mRNA and rRNA. rRNA is 17-42 times more abundant than mRNA (Deng *et al*., 2022). It is possible that the general increase in m^6A labeling observed with m^6A-targeting antibodies reflects increased m^6A methylation of rRNA occurring in a DRACH-independent context that could mask a general decrease in m^6A labeling of mRNA (Jiang *et al*., 2021). Indeed, rRNA-specific m^6A writers METTL5 and ZCCHC4 respectively methylate at positions A1832 and A4220, which occur outside of DRACH motifs (Ma *et al*., 2019; Van Tran *et al*., 2019). The observations from this study provide the necessary granular detail for the human brain mRNA transcriptome that identifies a distinct, robust age-related regulation of m^6A in normal Control subjects that contrasts with dysregulation in AD subjects.

The current study has inherent limitations to consider. First, DART constructs are limited by the YTH binding capacity and restricted to m^6A site identification within DRACH motifs. Although most m^6A sites on mRNA occur within the DRACH context (Schwartz *et al*., 2014), non-DRACH m^6A sites exist, which can be detected by other methods such as GLORI-seq (Liu *et al*., 2023). If scDART methods are developed for use with frozen tissue, studies of cellular

heterogeneity become possible; such methods are currently available for use *in vitro* (Tegowski, Flamand, & Meyer, 2022) and *in vivo* (Tegowski *et al*., 2024). Second, we did not observe a strong m^6A site enrichment around the stop codon (**Fig. 1C**), which is typically present (Olarerin-George & Jaffrey, 2017). However, our m^6A site distribution is similar to what prior DART-seq studies reported (Flamand & Meyer, 2022; McMillan *et al*., 2023). Differences in m^6A sequencing technique (e.g., DART-seq versus MeRIP-seq), species (e.g. human versus mouse), and sample quality (e.g., cell lysate versus flash frozen tissue) could impact the m^6A site distribution. Third, the cohort size of n=19/group is sufficient to power a strong study characterizing changes in m^6A labeling in AD, but insufficient to capture variation among related disorders, dementia subtypes, genetic risk factors (e.g., *APOE* variance, PS1 mutations impacting Aβ production, TREM2 levels impacting neuroinflammation), ancestry, and sex (Knopman *et al*., 2021). The biology of m^6A extends into direct readers, including YTHDF1/2/3, IGF2BP1/2/3, and neurodegeneration-linked indirect readers, including FMRP, HNRNPA2B1, and TDP-43; investigating disease related changes in these readers will provide insight into factors controlling synaptic localization and/or translation of m^6A-modified transcripts.

The results presented in this study demonstrate a striking response of RNA metabolism to the pathophysiology of AD, and delineate how RNA modifications, especially m^6A, might alter RNA metabolism in the brain with respect to age and disease. We uncovered a strong 3'UTR m^6A component in normal aging, a global reduction of m^6A-modified transcripts in AD, and two m^6A-associated dysregulated axes at tripartite synapses and proteostasis. The results provide granularity to m^6A methylation that was previously unknown, such as with site-specific differential changes in AD. Knowing the specific m^6A methylation changes occurring with AD could lead to future approaches that clarify disease heterogeneity as well as engineered approaches to reverse m^6A modifications in specific gene targets selected for the role in the pathophysiology of AD.

MATERIALS AND METHODS

Tissue samples

Brain tissues were obtained from the University of Kentucky Alzheimer's Disease Research Center (UK-ADRC) at the Sanders Brown Center on Aging. Methods for recruitment and pathological workup of these cases have been described previously (Schmitt *et al*., 2021; Nelson *et al*., 2023). Dorsolateral prefrontal cortex (Broadman area 9) samples from Control and AD cases using pathological criteria for group designation (Hyman *et al*., 2012; n=19/group) were used in this study. The demographics, clinical, and neuropathological characteristics and post-mortem intervals (PMI) of the cases are presented in Table 1. The Control and AD cohorts were matched for age, sex, PMI, and RNA quality.

Tissue homogenization and RNA extraction

Brain tissue was cut into ~50mg pieces on dry ice. The tissue was then wrapped in tin foil, placed over a metal block half submerged in liquid nitrogen, pulverized by a hammer, and placed into a lysing tube (Fisher Scientific, #MP116913100). 1 mL of Qiazol (Qiagen, #79306) was added to each tube. Tissue was homogenized by a bead mill (Fisherbrand™, #15-340-163) for 40 s at 4 ^{o}C and then sat at room temperature for 5 minutes. 200 µL of chloroform was then added, tubes were shaken vigorously for 60 s, and then rested again at room temperature for 3 minutes. Samples were centrifuged for 15 minutes at 4 ^{o}C for 12,000 x g to separate the organic, middle, and aqueous phase. The aqueous phase was carefully transferred to a gDNA eliminator column (Qiagen, part of RNeasy Plus kit) and spun at 8000 x g for 15 s. The spun phase was then mixed with 70% EtOH and transferred to a spin column. The RNA purification steps were subsequently carried out as described using the RNeasy Plus kit with DNase I treatment (Qiagen, #74136). After elution with 40 µL RNase-free water, RNA was quantified and assessed for

quality on the Agilent TapeStation 4200 using the RNA ScreenTape assay and for purity on the Nanodrop.

DART enzyme preparation and quantification

DART enzyme sequences (pCMV-APOBEC1-YTH [Addgene, #131636] and pCMV-APOBEC1-YTH^{mut} [Addgene, #131637]) were cloned into the pET-His6-MBP vector (Addgene, #29656, a gift from Kate Meyer). A glycerol stab of Rosetta™ 2 (DE3) pLysS Singles™ Competent Cells (Sigma Aldrich, #71402) was transformed with DART-enzyme expression vectors and grown in Terrific Broth (Thermo Fisher, #22711022, supplemented with 50 µg/mL Kanamycin) overnight at 37 °C with shaking at 200 rpm. The following day, 1 mL of starter culture was added to 90 mL of Boca Scientific Inc. Terrific Broth Auto-Induction Medium (Fisher Scientific, #NC1894479, supplemented with 50 µg/mL Kanamycin) and incubated for 7 hours at 37 °C with shaking at 200 rpm. Then, the cells were placed at 18 °C overnight with shaking at 200 rpm. Finally, the bacteria cultures were spun down at 6000 x g for 10 minutes at 4 °C, and the cell pellet was stored at -80°C until further use. The cell pellet was lysed using the EasyPrep Bacterial Protein Extraction Kit (Cepham, #10450). After thawing on ice for 30 minutes, 10 mL of lysis buffer (0.2% lysozyme, 2% nuclease) was added, and cells were homogenized and incubated for 30 minutes with mixing every 5-10 minutes. Cell debris was spun down at 12,500 x g for 1 hour at 4 °C to obtain a cleared protein extract. The protein extract was purified using the HiTrap Chelating columns (Cytiva Life Sciences, #17040901) on the Äkta pure™ chromatography system (Cytiva Life Sciences). All steps were carried out using DEPC-treated water. HiTrap Chelating columns were first flushed with water, charged with 0.1 M cobalt(II) chloride, equilibrated with an equilibrium buffer (50 mM Na2HPO4, 100 mM NaCl, 10 mM imidazole, pH 7.4), and loaded with protein extract by a circulating pump following the manufacturer's instructions. Next, the columns were washed with wash buffer (10 mM Hepes, 300 mM NaCl, 10 mM imidazole, pH 7.4), and the enzymes were eluted with a linear gradient from 15% to 55% of elution buffer (10 mM Hepes, 1 M NaCl, 300 mM imidazole, pH 7.4) using the Äkta pureTM system. Finally, purified enzyme was dialyzed using Slide-A-Lyzer Dialysis Cassettes (20,000 MWCO; ThermoScientific, #66012) in dialysis buffer (10 mM Tris-HCl, 100 mM NaCl, DTT, pH 7.4), mixed with glycerol to obtain a 20% glycerol solution, snapped frozen,

and stored at -80 °C until further use. Protein purity and concentration were assessed against a BSA standard curve using SDS-PAGE followed by Coomassie stain.

DART reaction and RNA repurification

DART reactions were performed as previously described (Zhu *et al.*, 2022). A 50 µL reaction was set up in a 200 µL PCR tube (5 µL 10x DART buffer [100 mM Tris-HCL (pH 7.4), 500 mM KCl, 1 µM $ZnCl_2$], 1 µL RNasin® Ribonuclease Inhibitor [40 U/µL, Promega, #N2615], 50 ng of total purified RNA, 250 ng of purified DART protein [either APOBEC1-YTH or APOBEC-YTH^{mut}], molecular grade RNase-free water to 50 µL). Tubes were gently mixed by tapping, briefly spun, and added to a pre-heated thermal cycler at 37 ^{o}C for 4 hours. After incubation, RNA was purified using the RNeasy Micro Kit (Qiagen, #74004) according to the manufacturer's instructions and eluted with 14 µL of molecular grade RNase-free water. RNA was quantified and assessed for quality on the Agilent TapeStation 4200 using the High Sensitivity RNA ScreenTape assay.

cDNA synthesis, DART PCR, and editing quantification from Sanger sequencing

cDNA was generated with the SuperScript III Reverse Transcriptase kit (Invitrogen, #18080044) using 3 ng of repurified DART-enzyme-treated total RNA as input and 50 ng of random hexamer primers for amplification (Thermo Scientific, #N8080127). PCR was performed with AmpliTaq Gold® 360 Master Mix (Applied Biosystems, #4398881) using 1 µL of cDNA and 1.0 µM of forward and reverse gene-specific primers (list below). PCR products were sent to Quintara Biosciences for purification and Sanger sequencing. Percent C>U conversion was quantified using EditR (Kluesner *et al.*, 2018).

DART PCR primers

The *ACTB* primers were from a previous study (Tegowski, Flamand, & Meyer, 2022). The *GABRA1* 3'UTR primers were designed in 4 sets to capture the 7 detected m^{6}A sites by DART-seq (***see Table 2***).

Gene	**Forward (*5' → 3'*)**	**Reverse (*5' → 3'*)**
ACTB	CAACACAGTGCTGTCTGGC	GCCATGCCAATCTCATCTTG
GABRA1	TGACAGAGCAAGCGAAAGAG	GGGGATCTTCAGCTTTGGAAC

3'UTR 1		
GABRA1 3'UTR 2	GCCCAACACTCACTTAATTCTCA	GGAATGACTTGAACAGAGAGCA
GABRA1 3'UTR 3	CAGTTGCTCTCTGTTCAAGTCA	TGGGCAGTAATGAAACAGACTAG
GABRA1 3'UTR 4	ACTTCTCATGGCTAACTTTTGGT	CATCTGCCATAAACAACCTTGAT

cDNA library synthesis and sequencing processing

3 ng of total RNA was amplified to create cDNA libraries using the SMARTer® Stranded Total RNA-Seq Kit v2 (Takara Bio, #634411) following the manufacturer's protocol. Libraries were generated for all n=38 APOBEC-YTH-treated samples, while only a half of the libraries were generated for APOBEC-YTH^{mut}-treated samples: C5, C7, C8, C10, C11, C12, C15-C19, A4-6, A8, A10-13, A15, A16, and A18 (***see Table 1***). cDNA library quality, appropriate fragment size (300-400 bp), and concentration were determined using the Agilent TapeStation 4200 and D1000 ScreenTape Assay. The cDNA libraries were normalized and pooled at a concentration that achieved >20,000,000 unique reads per sample and run on the Illumina Next-seq 2000 (100 cycles with 50 x 50 paired ends) by the Microarray and Sequencing Resources Facility at Boston University Medical Center to generate 1.2 billion total reads.

Fastq files from the DART reactions were obtained from BaseSpace Illumina. Quality control (QC) of the sequence data was performed using FastQC (v0.12.1) which assessed read quality, GC content, duplication levels, and adaptor contamination (Andrews, 2010). Reads passing initial QC were aligned to the human reference genome (GRCh38.111) using STAR (version 2.7.9a)/ This mapped sequencing reads to the reference genome using single-pass alignment, generating sorted BAM files for downstream analysis (Dobin *et al*., 2013). The resulting BAM files for each sample contained mapped paired-end reads and a corresponding alignment report file. Gene and isoform levels were quantified using RSEM (version 1.3.1; Li & Dewey, 2011) and Bowtie2 (version 2.3.4.1; Langmead & Salzberg, 2012) and then annotated using Homo sapiens GRCh38.111.gtf annotation files. For each sample, this process generated gene-level files containing gene ID, length, effective length, expected count, CPM, and FPKM,

which were then combined across samples based on gene IDs for downstream analysis. 'Batch effects in the quantified gene expression data were assessed using principal component analysis (PCA)

m^6A site identification by C>U editing and visualization

The Bullseye pipeline was used to identify m^6A-modified sites (i.e., C>U editing, (Flamand & Meyer, 2022; Tegowski, Flamand, & Meyer, 2022; Zhu *et al*., 2022; Tegowski *et al*., 2024). First, the parseBAM.pl script was used to parse the sequences from the coordinate-sorted BAM files. Then, a matrix containing the number of A, T, G, C, and N at all positions with a minimum coverage of 10 reads was created for each APOBEC-YTH-treated sample. For APOBEC1-YTH^{mut}-treated samples, all BAM files were merged using Samtools and parsed as a reference matrix. The Find_edit_site.pl script was then used to find C>U mutations by comparing each APOBEC1-YTH sample to the APOBEC-YTH^{mut} reference matrix. We defined true, high-confident m^6A sites for each sample if a minimum number of C>U mutation events at a particular site was 2, the site had an editing ratio (i.e., C>U site counts/total site counts) between 0.10-0.95, and the APOBEC1-YTH editing ratio enrichment over APOBEC1-YTH^{mut} editing ratio was at least 1.5 times higher. Finally, sense C>U (and antisense G>A) transitions were filtered for presence of the surrounding DRACH motif using custom scripts and the GenomicRanges (10.18129/B9.bioc.GenomicRanges), BSgenome (10.18129/B9.bioc.BSgenome), Biostrings (10.18129/B9.bioc.Biostrings), and gUtils R packages (Lawrence *et al*., 2013; Pages *et al*., 2013).

Genomic features corresponding to m^6A modifications were first imported from a BED file generated using Bullseye results, employing the Guitar package (Cui *et al*., 2016). A comprehensive transcriptome annotation for Homo sapiens (GRCh38.111) was generated from a GTF file via the makeTxDbFromGFF function. The spatial distribution of m^6A sites along mRNA transcripts was subsequently visualized using the GuitarPlot function (***see Fig. 1C***). This approach mapped the input BED file to transcriptomic landmarks with a focus on both 5′ and 3′ regions, as indicated by the headOrtail parameter, and normalized the data by scaling each m^6A site to a relative position (0–1 range) within transcript regions to account for region length, and by applying site-specific weights based on transcript-level overlap and ambiguity to ensure accurate regional enrichment. Custom filtering (mapFilterTranscript = TRUE) was applied to

ensure precise localization of features, and the plot aesthetics were refined to enhance the interpretability of the resulting visualization.

For enrichment analysis of DRACH motif (***see Fig. S3A***), background sequences were generated by shuffling the input BED coordinates and extracting both target and background sequences from the human genome (GRCh38.111) using bedtools. HOMER (Heinz *et al*., 2010) tools were then applied—using findMotifs.pl for motif detection and annotatePeaks.pl with findMotifsGenome.pl for peak annotation—to identify enriched customized motifs in the target regions relative to the background.

Gene expression analysis and visualization

Differential expression analysis was conducted using the DESeq2 package in R (Love, Huber, & Andrews, 2014). Initially, raw count data were imported and subjected to a filtering step wherein only those genes exhibiting counts ≥10 in at least 19 samples were retained. Count normalization was subsequently performed using counts per million (CPM) to adjust for library size differences. To mitigate the influence of confounding variables, covariates including pre-extraction RNA integrity number (pre_dart_RIN), age, sex, and post-mortem interval (PMI) were incorporated into the model. The final design formula was specified as ~ pre_dart_RIN + Age + sex_num + PMI + AD_Ctr, with AD_Ctr representing the binary classification of AD versus Control. Differentially expressed genes (DEGs) between the AD and Control groups were determined using the Wald test; DEGs with an adjusted p-value (padj) ≤ 0.05 were deemed statistically significant.

To evaluate the similarity between our data and publicly available MSBB datasets, we computed Spearman correlations between the mean gene expression levels in our dataset and those across the BM 10 MSBB dataset (https://adknowledgeportal.org/). The MSSB data were generated from post-mortem brain tissue collected through the Mount Sinai VA Medical Center Brain Bank and were provided by Dr. Eric Schadt from Mount Sinai School of Medicine. We first calculated log2 counts per million (log2 CPM) using EdgeR (Kluesner *et al*., 2018), identified shared genes, extracted their log-transformed expression values, and performed correlation analysis. The results, including correlation coefficients and p-values, were visualized using scatter plots with fitted regression lines (***see Fig. 2C***).

PCA and volcano plots for DMGs and DEGs were generated in R using the ggplot2 package (Wickham, 2011). KEGG pathway analysis was performed using ShinyGo (Kanehisa & Goto, 2000; Luo & Brouwer, 2013; Ge, Jung, & Yao, 2020). GSEA was performed and visualized with dot plots and a network plot in R using the clusterProfiler package (Yu *et al*., 2012; Wu *et al*., 2021). Heatmaps for DAS and genes with overlapping DART-seq and RNA-seq GSEA terms were generated in R using the ComplexHeatmap package (Gu, Eils, & Schlesner, 2016; Gu, 2022).

Synaptosome isolation, BCA assay, and protein normalization

Synaptosome isolation was performed using Syn-PER™ Synaptic Protein Extraction Reagent (Thermo Scientific, #87793) following the manufacturer's protocol. Briefly, ~50 mg of brain tissue was dounced in Syn-PER Reagent supplemented with 1x of Halt™ Protease and Phosphatase Inhibitor Cocktails (100x, Thermo Scientific, #78440) on ice with ~10 slow strokes. The homogenate was transferred to a 1.7 mL microcentrifuge tube and spun at 1200 x g for 10 minutes at 4 ^{o}C. Supernatant was collected and the spin was repeated. Then, 20% of the supernatant was saved as the homogenate fraction and the other 80% was placed in a new 1.7mL tube and centrifuged at 15,000 x g for 20 minutes at 4 ^{o}C. The supernatant (i.e., cytosolic fraction) was saved and the pellet containing the synaptosomal fraction was resuspended in Syn-PER at 20% of the original volume used. Then, the fractions were quantified using the Pierce™ BCA Protein Assay Kit (Thermo Scientific, #23225 and #23227) according to the manufacturer's protocol. Absorbance was measured using the SpectraMax i3x Platform. Protein stocks were normalized across all samples to achieve the same concentration and volume after adding 1x Bolt™ Sample Reducing Agent (10x, Invitrogen, #B0009) and 1x of Bolt™ LDS Sample Buffer (4x, Invitrogen, #B0007). Finally, samples were boiled for 10 minutes at 95 ^{o}C and stored at -20 ^{o}C until use.

Immunoblot

Homogenate and synaptosomal fractions (3-10 µg, see table below) were loaded into a 4-15% Criterion™ TGX Stain-Free™ Protein Gel (Bio-Rad, #5678085) and were run using 1x Bolt MES SDS Running Buffer (20x, Life Technologies, #B0002). Afterwards, the gel was scanned using the Bio-Rad ChemiDoc™ XRS+ imager to obtain total protein bands for densitometry normalization. The gel was transferred to a PDVF membrane using the iBlot 2

System (Thermo Fisher Scientific) template #1. Once transferred, the membrane was blocked in Tris-buffered saline + 0.05% Tween (TBST) with 5% non-fat dry milk for 60 minutes shaking gently at room temperature. The membrane was then incubated in primary antibody overnight (list below) shaking gently at 4 ^{o}C in a solution of either TBST +1% BSA or phosphate buffered saline + 0.05% Tween (PBST) + 1% BSA (see table below). After 24 hours, the membranes were washed 3 times in TBST or PBST for 5 minutes each, shaking gently at room temperature. Then, the membranes were incubated in secondary antibody in TBST or PBST for 60 minutes shaking gently at room temperature. Secondary antibody solution was removed and membranes were washed 3 more times in TBST or PBST for 5 minutes each with gentle shaking at room temperature. Afterwards, membranes were incubated for ~15-30 seconds in Super Signal West Pico PLUS stable peroxide and luminol/enhancer (Thermo Scientific, #34580) and then imaged using the Bio-Rad ChemiDoc^{TM} XRS+ system. Densitometry quantification of images was performed using ImageJ.

Antibodies

Target	**Host species**	**Dilution**	**Solution**	**Protein (µg)**	**Company**	**Catalog #**
CAMK2A	Mouse	1:1000	TBST	10	Cell Signaling	50049S
SYP1	Rabbit	1:1000	TBST	10	Abcam	ab52636
B-Actin	Mouse	1:20,000	TBST	10	Millipore Sigma	MAB1501
G3BP1	Mouse	1:1000	TBST	10	ProteinTech	66486-1-Ig
Tau13	Mouse	1:10,000	PBST	3.75	Gift from Nicholas Kanaan	RRID: AB 2721193
4G8	Mouse	1:1000	PBST	3.75	BioLegend	800701
GABRA1	Rabbit	1:1000	TBST	5	ProteinTech	12410-1-AP
IgG (H+L) highly cross-absorbed secondary	Mouse	1:10,000	1° antibody solution		Invitrogen	A16017

antibody, HRP						
IgG (H+L) cross-absorbed secondary antibody, HRP	Rabbit	1:10,000	1° antibody solution		Invitrogen	31458

GABRA1 qPCR

Following RNA extraction, 1 µg of total RNA was amplified into cDNA using the High-Capacity cDNA Reverse Transcription Kit (Thermo Fisher Scientific, #4368814). cDNA was prepared for qPCR using Ssoadvanced™ Universal SYBR Green (Bio-Rad #1725270) and gene-specific primers (list below). Ct levels of *GABRA1* were normalized to Ct levels of *GAPDH* and fold change was determined using the $2^{-\Delta\Delta CT}$ method (Livak & Schmittgen, 2001).

qPCR primers

Gene	**Forward (*5' → 3'*)**	**Reverse (*5' → 3'*)**
GABRA1	AGACCAAGTGAGTGAGAGGC	AATCGTGGAGAGACTGGAGC
GAPDH	CTGACTTCAACAGCGACACC	GTGGTCCAGGGGTCTTACTC

Statistical analysis and figure generation

Statistical analyses were performed in GraphPad/Prism 10.1.2. Anderson-Darling, D'Agostino, Shapiro-Wilk, and Kolmogorov-Smirnov tests for normality were performed on all comparisons. If at least half of the tests were significant, the data were considered normally distributed. Unpaired t-tests were used for comparing normally distributed means of 2 groups. Otherwise, Mann-Whitney tests were performed. One-way or two-way ANOVAs, followed by Tukey's HSD post hoc analyses, were used for comparing normally distributed means of 3 or 3+ groups. Otherwise, Kruskal-Wallis tests followed by Tukey's HSD post hoc analyses were

performed. For all tests, p-value was set to 0.05 and mean ± standard deviation was reported. Results were visualized in GraphPad/Prism 10.1.2 or in R. Workflow illustrations were made with Biorender (Popoli *et al*., 2012).

ACKNOWLEDGEMENTS

This work was supported by funds to BW (NIH AG080810, AG072577, AG082665 and AG064932) and to JL (NIH AG090051). The brain banks were supported by grants from NIH to the UK ADRC (P30 AG072946) and to the BU ADRC (P30AG072978, U01NS086659, and U54NS115266).

CONFLICT OF INTEREST

BW is Co-founder and CSO of Aquinnah Pharmaceuticals Inc.

REFERENCES

Ainani, H., Bouchmaa, N., Mrid, R. B., & El Fatimy, R. (2023). Liquid-liquid phase separation of protein tau: An emerging process in Alzheimer's disease pathogenesis. *Neurobiology of disease*, *178*, 106011.

Alarcón, C. R., Goodarzi, H., Lee, H., Liu, X., Tavazoie, S., & Tavazoie, S. F. (2015). HNRNPA2B1 is a mediator of m6A-dependent nuclear RNA processing events. *Cell*, *162*(6), 1299-1308.

Anders, M., Chelysheva, I., Goebel, I., Trenkner, T., Zhou, J., Mao, Y., ... & Ignatova, Z. (2018). Dynamic m6A methylation facilitates mRNA triaging to stress granules. *Life science alliance*, *1*(4).

Andrews, S. (2010). FastQC: a quality control tool for high throughput sequence data. *(No Title)*.

Apicco, D. J., Ash, P. E., Maziuk, B., LeBlang, C., Medalla, M., Al Abdullatif, A., ... & Wolozin, B. (2018). Reducing the RNA binding protein TIA1 protects against tau-mediated neurodegeneration in vivo. *Nature neuroscience*, *21*(1), 72-80.

Apicco, D. J., Zhang, C., Maziuk, B., Jiang, L., Ballance, H. I., Boudeau, S., ... & Wolozin, B. (2019). Dysregulation of RNA splicing in tauopathies. *Cell reports*, *29*(13), 4377-4388.

Ash, P. E., Lei, S., Shattuck, J., Boudeau, S., Carlomagno, Y., Medalla, M., ... & Wolozin, B. (2021). TIA1 potentiates tau phase separation and promotes generation of toxic oligomeric tau. *Proceedings of the National Academy of Sciences*, *118*(9), e2014188118.

Atrian, F., Ramirez, P., De Mange, J., Marquez, M., Gonzalez, E. M., Minaya, M., ... & Frost, B. (2024). m6A-dependent circular RNA formation mediates tau-induced neurotoxicity. *bioRxiv*.

Baltan, S. (2014). Excitotoxicity and mitochondrial dysfunction underlie age-dependent ischemic white matter injury. *Glutamate and ATP at the Interface of Metabolism and Signaling in the Brain*, 151-170.

Baughn, M. W., Melamed, Z. E., López-Erauskin, J., Beccari, M. S., Ling, K., Zuberi, A., ... & Cleveland, D. W. (2023). Mechanism of STMN2 cryptic splice-polyadenylation and its correction for TDP-43 proteinopathies. *Science*, *379*(6637), 1140-1149.

Brewer, L. D., Thibault, O., Staton, J., Thibault, V., Rogers, J. T., Garcia-Ramos, G., ... & Porter, N. M. (2007). Increased vulnerability of hippocampal neurons with age in culture: temporal association with increases in NMDA receptor current, NR2A subunit expression and recruitment of L-type calcium channels. *Brain research*, *1151*, 20-31.

Carello-Collar, G., Bellaver, B., Ferreira, P. C., Ferrari-Souza, J. P., Ramos, V. G., Therriault, J., ... & Zimmer, E. R. (2023). The GABAergic system in Alzheimer's disease: a systematic review with meta-analysis. *Molecular psychiatry*, *28*(12), 5025-5036.

Castro-Hernández, R., Berulava, T., Metelova, M., Epple, R., Peña Centeno, T., Richter, J., ... & Fischer, A. (2023). Conserved reduction of m6A RNA modifications during aging and neurodegeneration is linked to changes in synaptic transcripts. *Proceedings of the National Academy of Sciences*, *120*(9), e2204933120.

Cui, X., Wei, Z., Zhang, L., Liu, H., Sun, L., Zhang, S. W., ... & Meng, J. (2016). Guitar: an R/bioconductor package for gene annotation guided transcriptomic analysis of RNA□related genomic features. *BioMed research international*, *2016*(1), 8367534.

De Conti, L., Baralle, M., & Buratti, E. (2017). Neurodegeneration and RNA□binding proteins. *Wiley Interdisciplinary Reviews: RNA*, *8*(2), e1394.

Deng, Z. L., Münch, P. C., Mreches, R., & McHardy, A. C. (2022). Rapid and accurate identification of ribosomal RNA sequences via deep learning. *Nucleic acids research*, *50*(10), e60-e60.

Dobin, A., Davis, C. A., Schlesinger, F., Drenkow, J., Zaleski, C., Jha, S., ... & Gingeras, T. R. (2013). STAR: ultrafast universal RNA-seq aligner. *Bioinformatics*, *29*(1), 15-21.

Dobra, I., Pankivskyi, S., Samsonova, A., Pastre, D., & Hamon, L. (2018). Relation between stress granules and cytoplasmic protein aggregates linked to neurodegenerative diseases. *Current neurology and neuroscience reports*, *18*, 1-9.

Dominissini, D., Moshitch-Moshkovitz, S., Salmon-Divon, M., Amariglio, N., & Rechavi, G. (2013). Transcriptome-wide mapping of N 6-methyladenosine by m6A-seq based on immunocapturing and massively parallel sequencing. *Nature protocols*, *8*(1), 176-189.

Dominissini, D., Moshitch-Moshkovitz, S., Schwartz, S., Salmon-Divon, M., Ungar, L., Osenberg, S., ... & Rechavi, G. (2012). Topology of the human and mouse m6A RNA methylomes revealed by m6A-seq. *Nature*, *485*(7397), 201-206.

Dong, X. X., Wang, Y., & Qin, Z. H. (2009). Molecular mechanisms of excitotoxicity and their relevance to pathogenesis of neurodegenerative diseases. *Acta Pharmacologica Sinica*, *30*(4), 379-387.

Edens, B. M., Vissers, C., Su, J., Arumugam, S., Xu, Z., Shi, H., ... & Ma, Y. C. (2019). FMRP modulates neural differentiation through m6A-dependent mRNA nuclear export. *Cell reports*, *28*(4), 845-854.

Fan, Y., Lv, X., Chen, Z., Peng, Y., & Zhang, M. (2023). m6A methylation: critical roles in aging and neurological diseases. *Frontiers in Molecular Neuroscience*, *16*, 1102147.

Feng, Y., Absher, D., Eberhart, D. E., Brown, V., Malter, H. E., & Warren, S. T. (1997). FMRP associates with polyribosomes as an mRNP, and the I304N mutation of severe fragile X syndrome abolishes this association. *Molecular cell*, *1*(1), 109-118.

Flamand, M. N., & Meyer, K. D. (2022). m6A and YTHDF proteins contribute to the localization of select neuronal mRNAs. *Nucleic acids research*, *50*(8), 4464-4483.

Flamand, M. N., Tegowski, M., & Meyer, K. D. (2023). The proteins of mRNA modification: writers, readers, and erasers. *Annual review of biochemistry*, *92*(1), 145-173.

Fu, Y., & Zhuang, X. (2020). m6A-binding YTHDF proteins promote stress granule formation. *Nature chemical biology*, *16*(9), 955-963.

Ge, S. X., Jung, D., & Yao, R. (2020). ShinyGO: a graphical gene-set enrichment tool for animals and plants. *Bioinformatics*, *36*(8), 2628-2629.

Gu, Z. (2022). Complex heatmap visualization. *Imeta*, *1*(3), e43.

Gu, Z., Eils, R., & Schlesner, M. (2016). Complex heatmaps reveal patterns and correlations in multidimensional genomic data. *Bioinformatics*, *32*(18), 2847-2849.

Han M, Liu Z, Xu Y, Liu X, Wang D, Li F, Wang Y, Bi J. Abnormality of m6A mRNA Methylation Is Involved in Alzheimer's Disease. Front Neurosci. 2020 Feb 28;14:98. doi: 10.3389/fnins.2020.00098. PMID: 32184705; PMCID: PMC7058666.

Heinz, S., Benner, C., Spann, N., Bertolino, E., Lin, Y. C., Laslo, P., ... & Glass, C. K. (2010). Simple combinations of lineage-determining transcription factors prime cis-regulatory elements required for macrophage and B cell identities. *Molecular cell*, *38*(4), 576-589.

Hsieh, Y. C., Guo, C., Yalamanchili, H. K., Abreha, M., Al-Ouran, R., Li, Y., ... & Shulman, J. M. (2019). Tau-mediated disruption of the spliceosome triggers cryptic RNA splicing and neurodegeneration in Alzheimer’s disease. *Cell reports*, *29*(2), 301-316.

Hsu, P. J., Shi, H., Zhu, A. C., Lu, Z., Miller, N., Edens, B. M., ... & He, C. (2019). The RNA-binding protein FMRP facilitates the nuclear export of N6-methyladenosine–containing mRNAs. *Journal of Biological Chemistry*, *294*(52), 19889-19895.

Hyman, B. T., Phelps, C. H., Beach, T. G., Bigio, E. H., Cairns, N. J., Carrillo, M. C., ... & Montine, T. J. (2012). National Institute on Aging–Alzheimer's Association guidelines for the neuropathologic assessment of Alzheimer's disease. *Alzheimer's & dementia*, *8*(1), 1-13.

Hynd, M. R., Scott, H. L., & Dodd, P. R. (2004). Glutamate-mediated excitotoxicity and neurodegeneration in Alzheimer’s disease. *Neurochemistry international*, *45*(5), 583-595.

Jiang, L., Ash, P. E., Maziuk, B. F., Ballance, H. I., Boudeau, S., Abdullatif, A. A., ... & Wolozin, B. (2019). TIA1 regulates the generation and response to toxic tau oligomers. *Acta neuropathologica*, *137*, 259-277.

Jiang, L., Lin, W., Zhang, C., Ash, P. E., Verma, M., Kwan, J., ... & Wolozin, B. (2021a). Interaction of tau with HNRNPA2B1 and N6-methyladenosine RNA mediates the progression of tauopathy. *Molecular cell*, *81*(20), 4209-4227.

Jiang, L., Roberts, R., Wong, M., Zhang, L., Webber, C. J., Libera, J., ... & Wolozin, B. (2024). β-amyloid accumulation enhances microtubule associated protein tau pathology in an APPNL-GF/MAPTP301S mouse model of Alzheimer’s disease. *Frontiers in Neuroscience*, *18*, 1372297.

Jiang, X., Liu, B., Nie, Z., Duan, L., Xiong, Q., Jin, Z., ... & Chen, Y. (2021b). The role of m6A modification in the biological functions and diseases. *Signal transduction and targeted therapy*, *6*(1), 74.

Kaehler, C., Isensee, J., Nonhoff, U., Terrey, M., Hucho, T., Lehrach, H., & Krobitsch, S. (2012). Ataxin-2-like is a regulator of stress granules and processing bodies. *PloS one*, *7*(11), e50134.

Kanehisa, M., & Goto, S. (2000). KEGG: kyoto encyclopedia of genes and genomes. Nucleic acids research, 28(1), 27-30.

Karapetyan, A. R., Buiting, C., Kuiper, R. A., & Coolen, M. W. (2013). Regulatory roles for long ncRNA and mRNA. *Cancers*, *5*(2), 462-490.

King, O. D., Gitler, A. D., & Shorter, J. (2012). The tip of the iceberg: RNA-binding proteins with prion-like domains in neurodegenerative disease. *Brain research*, *1462*, 61-80.

Kluesner, M. G., Nedveck, D. A., Lahr, W. S., Garbe, J. R., Abrahante, J. E., Webber, B. R., & Moriarity, B. S. (2018). EditR: a method to quantify base editing from Sanger sequencing. *The CRISPR journal*, *1*(3), 239-250.

Knopman, D. S., Amieva, H., Petersen, R. C., Chételat, G., Holtzman, D. M., Hyman, B. T., ... & Jones, D. T. (2021). Alzheimer disease. *Nature reviews Disease primers*, *7*(1), 33.

Langmead, B., & Salzberg, S. L. (2012). Fast gapped-read alignment with Bowtie 2. *Nature methods*, *9*(4), 357-359.

Lawrence, M., Huber, W., Pagès, H., Aboyoun, P., Carlson, M., Gentleman, R., ... & Carey, V. J. (2013). Software for computing and annotating genomic ranges. *PLoS computational biology*, *9*(8), e1003118.

Lee, G., Thangavel, R., Sharma, V. M., Litersky, J. M., Bhaskar, K., Fang, S. M., ... & Ksiezak-Reding, H. (2004). Phosphorylation of tau by fyn: implications for Alzheimer's disease. *Journal of Neuroscience*, *24*(9), 2304-2312.

Lester, E., Van Alstyne, M., McCann, K. L., Reddy, S., Cheng, L. Y., Kuo, J., ... & Parker, R. (2023). Cytosolic condensates rich in polyserine define subcellular sites of tau aggregation. *Proceedings of the National Academy of Sciences*, *120*(3), e2217759120.

Li, B., & Dewey, C. N. (2011). RSEM: accurate transcript quantification from RNA-Seq data with or without a reference genome. *BMC bioinformatics*, *12*, 1-16.

Li, Y., & Sun, S. (2025). RNA dysregulation in neurodegenerative diseases. *The EMBO Journal*, *44*(3), 613-638.

Li, Y., Dou, X., Liu, J., Xiao, Y., Zhang, Z., Hayes, L., ... & Sun, S. (2023). Globally reduced N 6-methyladenosine (m6A) in C9ORF72-ALS/FTD dysregulates RNA metabolism and contributes to neurodegeneration. *Nature neuroscience*, *26*(8), 1328-1338.

Limon, A., Reyes-Ruiz, J. M., & Miledi, R. (2012). Loss of functional GABAA receptors in the Alzheimer diseased brain. *Proceedings of the National Academy of Sciences*, *109*(25), 10071-10076.

Linder, B., Grozhik, A. V., Olarerin-George, A. O., Meydan, C., Mason, C. E., & Jaffrey, S. R. (2015). Single-nucleotide-resolution mapping of m6A and m6Am throughout the transcriptome. *Nature methods*, *12*(8), 767-772.

Ling, J. P., Pletnikova, O., Troncoso, J. C., & Wong, P. C. (2015). TDP-43 repression of nonconserved cryptic exons is compromised in ALS-FTD. *Science*, *349*(6248), 650-655.

Liu, C., Sun, H., Yi, Y., Shen, W., Li, K., Xiao, Y., ... & Wang, J. (2023). Absolute quantification of single-base m6A methylation in the mammalian transcriptome using GLORI. *Nature Biotechnology*, *41*(3), 355-366.

Liu, Y., & Shi, S. L. (2021). The roles of hnRNP A2/B1 in RNA biology and disease. *Wiley Interdisciplinary Reviews: RNA*, *12*(2), e1612.

Livak, K. J., & Schmittgen, T. D. (2001). Analysis of relative gene expression data using real-time quantitative PCR and the $2^{-\Delta\Delta CT}$ method. *methods*, *25*(4), 402-408.

López de Silanes, I., Galbán, S., Martindale, J. L., Yang, X., Mazan-Mamczarz, K., Indig, F. E., ... & Gorospe, M. (2005). Identification and functional outcome of mRNAs associated with RNA-binding protein TIA-1. *Molecular and cellular biology*, *25*(21), 9520-9531.

Love, M. I., Huber, W., & Anders, S. (2014). Moderated estimation of fold change and dispersion for RNA-seq data with DESeq2. *Genome biology*, *15*, 1-21.

Luo, W., & Brouwer, C. (2013). Pathview: an R/Bioconductor package for pathway-based data integration and visualization. *Bioinformatics*, *29*(14), 1830-1831.

Ma, H., Wang, X., Cai, J., Dai, Q., Natchiar, S. K., Lv, R., ... & He, C. (2019). N 6-Methyladenosine methyltransferase ZCCHC4 mediates ribosomal RNA methylation. *Nature chemical biology*, *15*(1), 88-94.

Ma, X. R., Prudencio, M., Koike, Y., Vatsavayai, S. C., Kim, G., Harbinski, F., ... & Gitler, A. D. (2022). TDP-43 represses cryptic exon inclusion in the FTD–ALS gene UNC13A. *Nature*, *603*(7899), 124-130.

Marrone, L., Drexler, H. C., Wang, J., Tripathi, P., Distler, T., Heisterkamp, P., ... & Sterneckert, J. (2019). FUS pathology in ALS is linked to alterations in multiple ALS-associated proteins and rescued by drugs stimulating autophagy. *Acta neuropathologica*, *138*, 67-84.

Martin, L., Latypova, X., Wilson, C. M., Magnaudeix, A., Perrin, M. L., & Terro, F. (2013). Tau protein phosphatases in Alzheimer's disease: the leading role of PP2A. *Ageing research reviews*, *12*(1), 39-49.

Martinez, F. J., Pratt, G. A., Van Nostrand, E. L., Batra, R., Huelga, S. C., Kapeli, K., ... & Yeo, G. W. (2016). Protein-RNA networks regulated by normal and ALS-associated mutant HNRNPA2B1 in the nervous system. *Neuron*, *92*(4), 780-795.

Masliah, E., Hansen, L., Alford, M., Deteresa, R., & Mallory, M. (1996). Deficient glutamate tranport is associated with neurodegeneration in Alzheimer's disease. *Annals of Neurology: Official Journal of the American Neurological Association and the Child Neurology Society*, *40*(5), 759-766.

Mayr, C. (2017). Regulation by 3′-untranslated regions. *Annual review of genetics*, *51*(1), 171-194.

Maziuk, B., Ballance, H. I., & Wolozin, B. (2017). Dysregulation of RNA binding protein aggregation in neurodegenerative disorders. *Frontiers in molecular neuroscience*, *10*, 89.

McIntyre, A. B., Gokhale, N. S., Cerchietti, L., Jaffrey, S. R., Horner, S. M., & Mason, C. E. (2020). Limits in the detection of m6A changes using MeRIP/m6A-seq. *Scientific reports*, *10*(1), 6590.

McMillan, M., Gomez, N., Hsieh, C., Bekier, M., Li, X., Miguez, R., ... & Barmada, S. J. (2023). RNA methylation influences TDP43 binding and disease pathogenesis in models of amyotrophic lateral sclerosis and frontotemporal dementia. *Molecular cell*, *83*(2), 219-236.

Merkurjev, D., Hong, W. T., Iida, K., Oomoto, I., Goldie, B. J., Yamaguti, H., ... & Wang, D. O. (2018). Synaptic N 6-methyladenosine (m6A) epitranscriptome reveals functional partitioning of localized transcripts. *Nature neuroscience*, *21*(7), 1004-1014.

Meur, S., & Karati, D. (2025). Fyn kinase in Alzheimer’s disease: Unraveling molecular mechanisms and therapeutic implications. *Molecular Neurobiology*, *62*(1), 643-660.

Meyer, K. D. (2019). DART-seq: an antibody-free method for global m6A detection. *Nature methods*, *16*(12), 1275-1280.

Meyer, K. D. (2019). m6A-mediated translation regulation. *Biochimica et Biophysica Acta (Bba)-Gene Regulatory Mechanisms*, *1862*(3), 301-309.

Meyer, K. D., & Jaffrey, S. R. (2017). Rethinking m6A readers, writers, and erasers. *Annual review of cell and developmental biology*, *33*(1), 319-342.

Mittag, T., & Parker, R. (2018). Multiple modes of protein–protein interactions promote RNP granule assembly. *Journal of molecular biology*, *430*(23), 4636-4649.

Montalbano, M., McAllen, S., Puangmalai, N., Sengupta, U., Bhatt, N., Johnson, O. D., ... & Kayed, R. (2020). RNA-binding proteins Musashi and tau soluble aggregates initiate nuclear dysfunction. *Nature Communications*, *11*(1), 4305.

Murakami, S., & Jaffrey, S. R. (2022). Hidden codes in mRNA: control of gene expression by m6A. *Molecular cell*, *82*(12), 2236-2251.

Nelson, R. S., Abner, E. L., Jicha, G. A., Schmitt, F. A., Di, J., Wilcock, D. M., ... & Nelson, P. T. (2023). Neurodegenerative pathologies associated with behavioral and psychological symptoms of dementia in a community-based autopsy cohort. *Acta Neuropathologica Communications*, *11*(1), 89.

Olarerin-George, A. O., & Jaffrey, S. R. (2017). MetaPlotR: a Perl/R pipeline for plotting metagenes of nucleotide modifications and other transcriptomic sites. *Bioinformatics*, *33*(10), 1563-1564.

Pages, H., Aboyoun, P., Gentleman, R., DebRoy, S., Pages, M. H., DataImport, D., ... & XStringSet-io, R. (2013). Package 'Biostrings'. *Bioconductor*, *18129*, 501.

Perlegos, A. E., Byrns, C. N., & Bonini, N. M. (2024). Cell type□specific regulation of m6A modified RNAs in the aging Drosophila brain. *Aging cell*, *23*(3), e14076.

Popoli, M., Yan, Z., McEwen, B. S., & Sanacora, G. (2012). The stressed synapse: the impact of stress and glucocorticoids on glutamate transmission. Nature Reviews Neuroscience, 13(1), 22-37.

Protter, D. S., & Parker, R. (2016). Principles and properties of stress granules. *Trends in cell biology*, *26*(9), 668-679.

Reineke, L. C., Kedersha, N., Langereis, M. A., van Kuppeveld, F. J., & Lloyd, R. E. (2015). Stress granules regulate double-stranded RNA-dependent protein kinase activation through a complex containing G3BP1 and Caprin1. *MBio*, *6*(2), 10-1128.

Richter, J. D., & Zhao, X. (2021). The molecular biology of FMRP: new insights into fragile X syndrome. *Nature Reviews Neuroscience*, *22*(4), 209-222.

Ries, R. J., Zaccara, S., Klein, P., Olarerin-George, A., Namkoong, S., Pickering, B. F., ... & Jaffrey, S. R. (2019). m6A enhances the phase separation potential of mRNA. *Nature*, *571*(7765), 424-428.

Ross, C. A., & Poirier, M. A. (2004). Protein aggregation and neurodegenerative disease. *Nature medicine*, *10*(Suppl 7), S10-S17.

Rudy, C. C., Hunsberger, H. C., Weitzner, D. S., & Reed, M. N. (2015). The role of the tripartite glutamatergic synapse in the pathophysiology of Alzheimer's disease. *Aging and disease*, *6*(2), 131.

Schmitt, F. A., Nelson, P. T., Abner, E., Scheff, S., A. Jicha, G., Smith, C., ... & Kryscio, R. J. (2012). University of Kentucky Sanders-Brown healthy brain aging volunteers: donor characteristics, procedures and neuropathology. *Current Alzheimer Research*, *9*(6), 724-733.

Schwartz, S., Mumbach, M. R., Jovanovic, M., Wang, T., Maciag, K., Bushkin, G. G., ... & Regev, A. (2014). Perturbation of m6A writers reveals two distinct classes of mRNA methylation at internal and 5′ sites. *Cell reports*, *8*(1), 284-296.

Shafik, A. M., Zhang, F., Guo, Z., Dai, Q., Pajdzik, K., Li, Y., ... & Jin, P. (2021). N6-methyladenosine dynamics in neurodevelopment and aging, and its potential role in Alzheimer's disease. *Genome biology*, *22*, 1-19.

Sikorski, V., Selberg, S., Lalowski, M., Karelson, M., & Kankuri, E. (2023). The structure and function of YTHDF epitranscriptomic m6A readers. *Trends in Pharmacological Sciences*, *44*(6), 335-353.

Sun, J., Cheng, B., Su, Y., Li, M., Ma, S., Zhang, Y., ... & Zhu, P. (2022). The potential role of m6A RNA methylation in the aging process and aging-associated diseases. *Frontiers in Genetics*, *13*, 869950.

Takahashi, K., Kong, Q., Lin, Y., Stouffer, N., Schulte, D. A., Lai, L., ... & Lin, C. L. G. (2015). Restored glial glutamate transporter EAAT2 function as a potential therapeutic approach for Alzheimer's disease. *Journal of experimental medicine*, *212*(3), 319-332.

Tegowski, M., & Meyer, K. D. (2022). Detection of m6A in single cultured cells using scDART-seq. *STAR protocols*, *3*(3), 101646.

Tegowski, M., & Meyer, K. D. (2024). Studying m6A in the brain: a perspective on current methods, challenges, and future directions. *Frontiers in Molecular Neuroscience*, *17*, 1393973.

Tegowski, M., Flamand, M. N., & Meyer, K. D. (2022). scDART-seq reveals distinct m6A signatures and mRNA methylation heterogeneity in single cells. *Molecular cell*, *82*(4), 868-878.

Tegowski, M., Prater, A. K., Holley, C. L., & Meyer, K. D. (2024). Single-cell m6A profiling in the mouse brain uncovers cell type-specific RNA methylomes and age-dependent differential methylation. *Nature neuroscience*, *27*(12), 2512-2520.

Tegowski, M., Zhu, H., & Meyer, K. D. (2022). Detecting m 6 A with In Vitro DART-Seq. *Post-transcriptional Gene Regulation*, 363-374.

Van Tran, N., Ernst, F. G. M., Hawley, B. R., Zorbas, C., Ulryck, N., Hackert, P., ... & Lafontaine, D. L. J. (2019). The human 18S rRNA m6A methyltransferase METTL5 is stabilized by TRMT112. *Nucleic acids research*, *47*(15), 7719-7733.

Vanderweyde, T., Apicco, D. J., Youmans-Kidder, K., Ash, P. E., Cook, C., da Rocha, E. L., ... & Wolozin, B. (2016). Interaction of tau with the RNA-binding protein TIA1 regulates tau pathophysiology and toxicity. *Cell reports*, *15*(7), 1455-1466.

Wang, I., Hennig, J., Jagtap, P. K. A., Sonntag, M., Valcárcel, J., & Sattler, M. (2014). Structure, dynamics and RNA binding of the multi-domain splicing factor TIA-1. *Nucleic acids research*, *42*(9), 5949-5966.

Weng, Y. L., Wang, X., An, R., Cassin, J., Vissers, C., Liu, Y., ... & Ming, G. L. (2018). Epitranscriptomic m6A regulation of axon regeneration in the adult mammalian nervous system. *Neuron*, *97*(2), 313-325.

Wickham, H. (2011). ggplot2. *Wiley interdisciplinary reviews: computational statistics*, *3*(2), 180-185.

Wolozin, B., & Apicco, D. (2014). RNA binding proteins and the genesis of neurodegenerative diseases. In *GeNeDis 2014: Neurodegeneration* (pp. 11-15). Cham: Springer International Publishing.

Wolozin, B., & Ivanov, P. (2019). Stress granules and neurodegeneration. *Nature Reviews Neuroscience*, *20*(11), 649-666.

Wu, B., Su, S., Patil, D. P., Liu, H., Gan, J., Jaffrey, S. R., & Ma, J. (2018). Molecular basis for the specific and multivariant recognitions of RNA substrates by human hnRNP A2/B1. *Nature communications*, *9*(1), 1-12.

Wu, T., Hu, E., Xu, S., Chen, M., Guo, P., Dai, Z., ... & Yu, G. (2021). clusterProfiler 4.0: A universal enrichment tool for interpreting omics data. *The innovation*, *2*(3).

Wu, Z., Lu, M., Liu, D., Shi, Y., Ren, J., Wang, S., ... & Liu, G. H. (2023). m6A epitranscriptomic regulation of tissue homeostasis during primate aging. *Nature Aging*, *3*(6), 705-721.

Yu, G., Wang, L. G., Han, Y., & He, Q. Y. (2012). clusterProfiler: an R package for comparing biological themes among gene clusters. *Omics: a journal of integrative biology*, *16*(5), 284-287.

Yu, J., Chen, M., Huang, H., Zhu, J., Song, H., Zhu, J., ... & Ji, S. J. (2018). Dynamic m6A modification regulates local translation of mRNA in axons. *Nucleic acids research*, *46*(3), 1412-1423.

Zaccara, S., & Jaffrey, S. R. (2020). A unified model for the function of YTHDF proteins in regulating m6A-modified mRNA. *Cell*, *181*(7), 1582-1595.

Zaccara, S., & Jaffrey, S. R. (2024). Understanding the redundant functions of the m6A-binding YTHDF proteins. *Rna*, *30*(5), 468-481.

Zhang, F., Kang, Y., Wang, M., Li, Y., Xu, T., Yang, W., ... & Jin, P. (2018). Fragile X mental retardation protein modulates the stability of its m6A-marked messenger RNA targets. *Human molecular genetics*, *27*(22), 3936-3950.

Zhang, W., Qian, Y., & Jia, G. (2021). The detection and functions of RNA modification m6A based on m6A writers and erasers. *Journal of Biological Chemistry*, *297*(2).

Zhao, F., Xu, Y., Gao, S., Qin, L., Austria, Q., Siedlak, S. L., ... & Zhu, X. (2021). METTL3-dependent RNA m 6 A dysregulation contributes to neurodegeneration in Alzheimer's disease through aberrant cell cycle events. Molecular neurodegeneration, 16, 1-25.

Zhu, H., Yin, X., Holley, C. L., & Meyer, K. D. (2022). Improved methods for deamination-based m6A detection. *Frontiers in Cell and Developmental Biology*, *10*, 888279.

Zhu, S., Shala, A., Bezginov, A., Sljoka, A., Audette, G., & Wilson, D. J. (2015). Hyperphosphorylation of intrinsically disordered tau protein induces an amyloidogenic shift in its conformational ensemble. *PLoS One*, *10*(3), e0120416.

Zou, Z., & He, C. (2024). The YTHDF proteins display distinct cellular functions on m6A-modified RNA. *Trends in Biochemical Sciences*.

Graphical Abstract

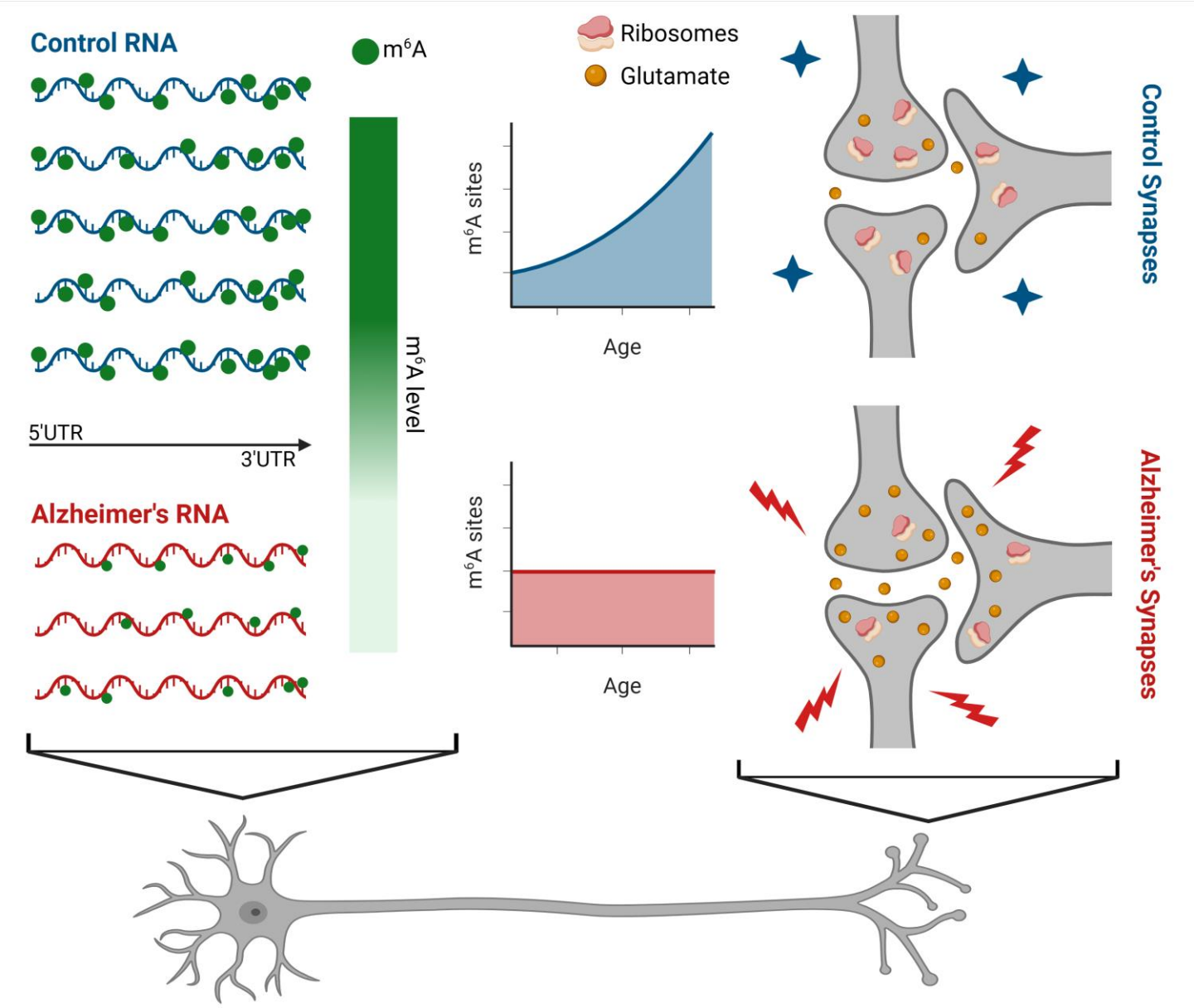

Figure 1

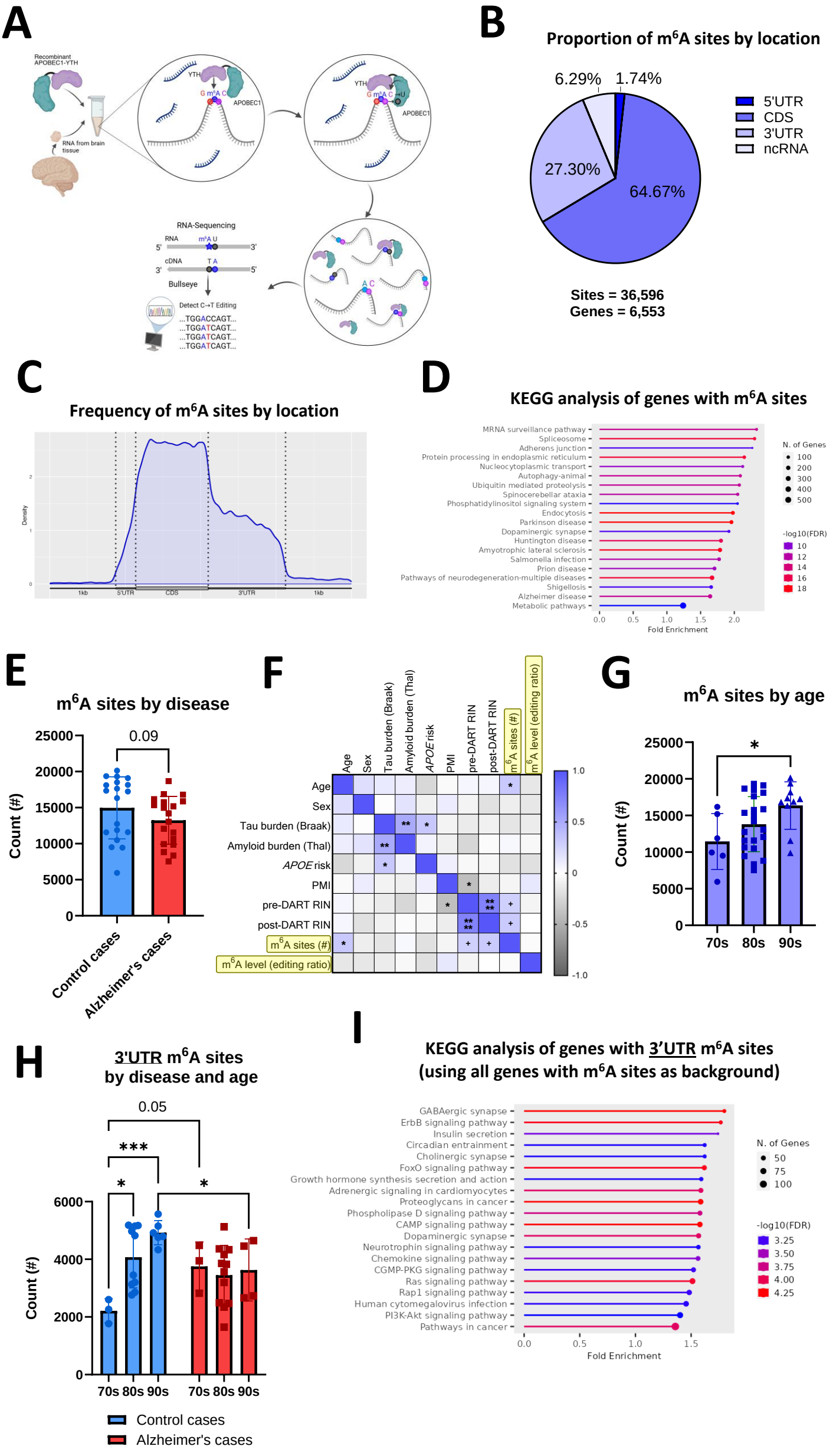
A
Recombinant APOBEC1-YTH
RNA from brain tissue
YTH
APOBEC1
RNA-Sequencing
RNA
cDNA
Bullseye
Detect C→T Editing
...TGGACCAGT...
...TGGATCAGT...
...TGGATCAGT...
...TGGATCAGT...
B
Proportion of m6A sites by location
6.29%
1.74%
27.30%
64.67%
5'UTR
CDS
3'UTR
ncRNA
Sites = 36,596
Genes = 6,553
C
Frequency of m6A sites by location
Density
1kb
5'UTR
CDS
3'UTR
1kb
D
KEGG analysis of genes with m6A sites
MRNA surveillance pathway
Spliceosome
Adherens junction
Protein processing in endoplasmic reticulum
Nucleocytoplasmic transport
Autophagy-animal
Ubiquitin mediated proteolysis
Spinocerebellar ataxia
Phosphatidylinositol signaling system
Endocytosis
Parkinson disease
Dopaminergic synapse
Huntington disease
Amyotrophic lateral sclerosis
Salmonella infection
Prion disease
Pathways of neurodegeneration-multiple diseases
Shigellosis
Alzheimer disease
Metabolic pathways
Fold Enrichment
N. of Genes
-log10(FDR)
E
m6A sites by disease
Count (#)
0.09
Control cases
Alzheimer's cases
F
Age
Sex
Tau burden (Braak)
Amyloid burden (Thal)
APOE risk
PMI
pre-DART RIN
post-DART RIN
m6A sites (#)
m6A level (editing ratio)
G
m6A sites by age
Count (#)
70s
80s
90s
H
3'UTR m6A sites by disease and age
0.05
***
Count (#)
70s 80s 90s
70s 80s 90s
Control cases
Alzheimer's cases
I
KEGG analysis of genes with 3'UTR m6A sites (using all genes with m6A sites as background)
GABAergic synapse
ErbB signaling pathway
Insulin secretion
Circadian entrainment
Cholinergic synapse
FoxO signaling pathway
Growth hormone synthesis secretion and action
Adrenergic signaling in cardiomyocytes
Proteoglycans in cancer
Phospholipase D signaling pathway
CAMP signaling pathway
Dopaminergic synapse
Neurotrophin signaling pathway
Chemokine signaling pathway
CGMP-PKG signaling pathway
Ras signaling pathway
Rap1 signaling pathway
Human cytomegalovirus infection
PI3K-Akt signaling pathway
Pathways in cancer
Fold Enrichment
N. of Genes
-log10(FDR)

Figure 2

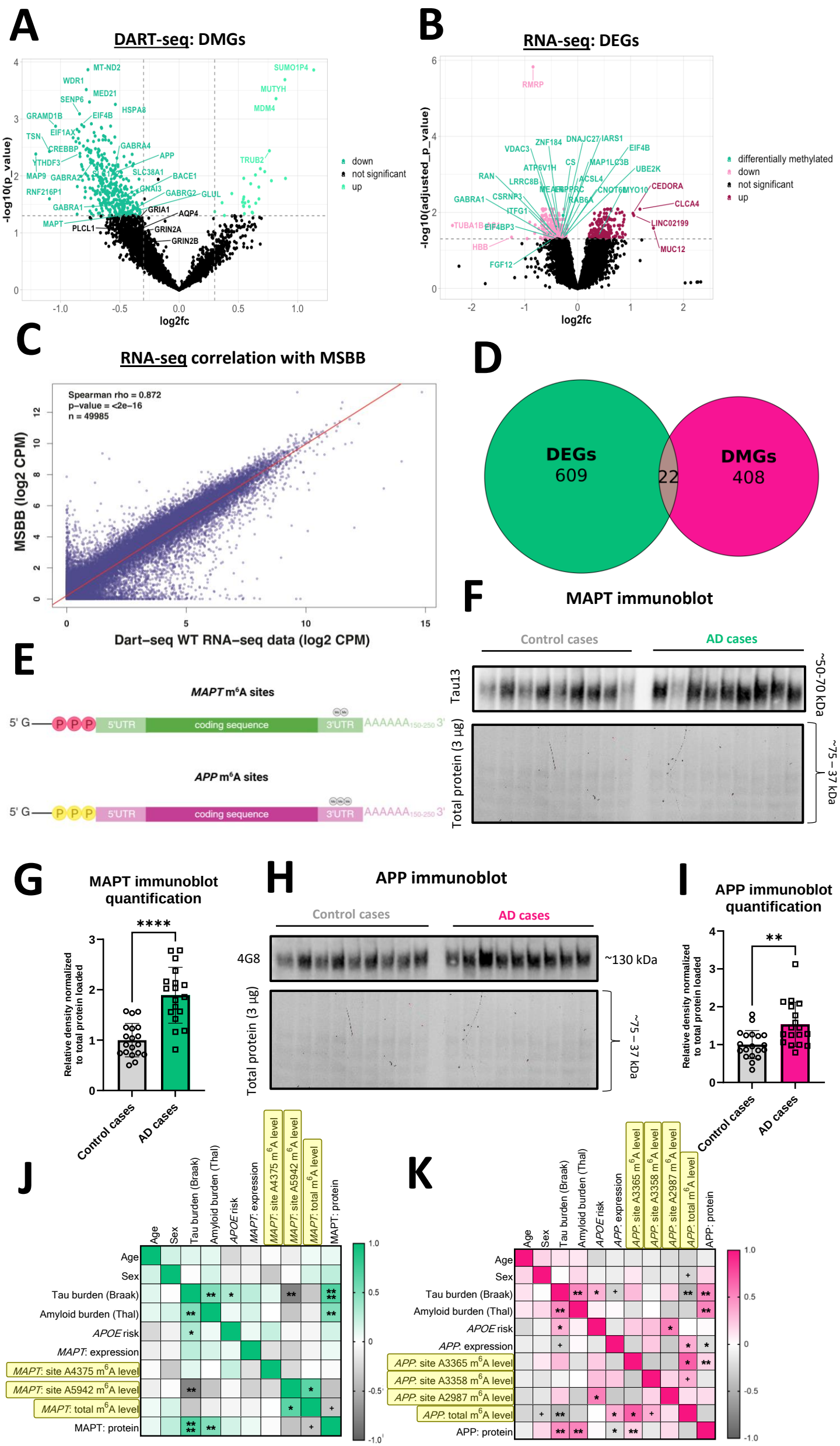
A
DART-seq: DMGs
-log10(p_value)
log2fc
down
not significant
up
MT-ND2
WDR1
MED21
SENP6
HSPA8
GRAMD1B
EIF4B
TSN
EIF1AX
CREBBP
GABRA4
APP
YTHDF3
MAP9
GABRA2
SLC38A1
BACE1
RNF216P1
GNAI3
GABRG2
GLUL
GABRA1
GRIA1
AQP4
MAPT
PLCL1
GRIN2A
GRIN2B
SUMO1P4
MUTYH
MDM4
TRUB2
B
RNA-seq: DEGs
-log10(adjusted_p_value)
log2fc
differentially methylated
down
not significant
up
RMRP
VDAC3
ZNF184
DNAJC27
IARS1
EIF4B
ATP6V1H
CS
MAP1LC3B
UBE2K
RAN
LRRC8B
ACSL4
CEDORA
GABRA1
CSRNP3
RAB6A
CLCA4
ITFG1
LINC02199
EIF4BP3
HBB
MUC12
FGF12
C
RNA-seq correlation with MSBB
Spearman rho = 0.872
p-value = <2e-16
n = 49985
MSBB (log2 CPM)
Dart-seq WT RNA-seq data (log2 CPM)
D
DEGs
609
22
DMGs
408
E
MAPT m6A sites
5' G
P P P
5'UTR
coding sequence
3'UTR
AAAAAA150-250 3'
APP m6A sites
F
MAPT immunoblot
Control cases
AD cases
Tau13
~50-70 kDa
Total protein (3 µg)
~75 – 37 kDa
G
MAPT immunoblot quantification
****
Relative density normalized to total protein loaded
Control cases
AD cases
H
APP immunoblot
Control cases
AD cases
4G8
~130 kDa
Total protein (3 µg)
~75 – 37 kDa
I
APP immunoblot quantification
**
Relative density normalized to total protein loaded
Control cases
AD cases
J
Age
Sex
Tau burden (Braak)
Amyloid burden (Thal)
APOE risk
MAPT: expression
MAPT: site A4375 m6A level
MAPT: site A5942 m6A level
MAPT: total m6A level
MAPT: protein
K
Age
Sex
Tau burden (Braak)
Amyloid burden (Thal)
APOE risk
APP: expression
APP: site A3365 m6A level
APP: site A3358 m6A level
APP: site A2987 m6A level
APP: total m6A level
APP: protein

Figure 3

A

DART-seq GSEA

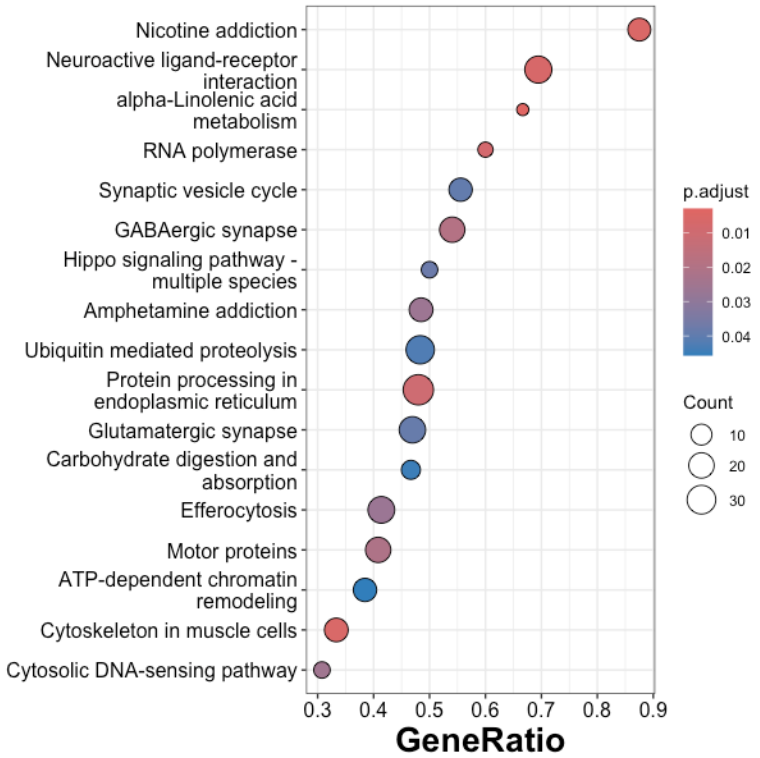

B

RNA-seq GSEA

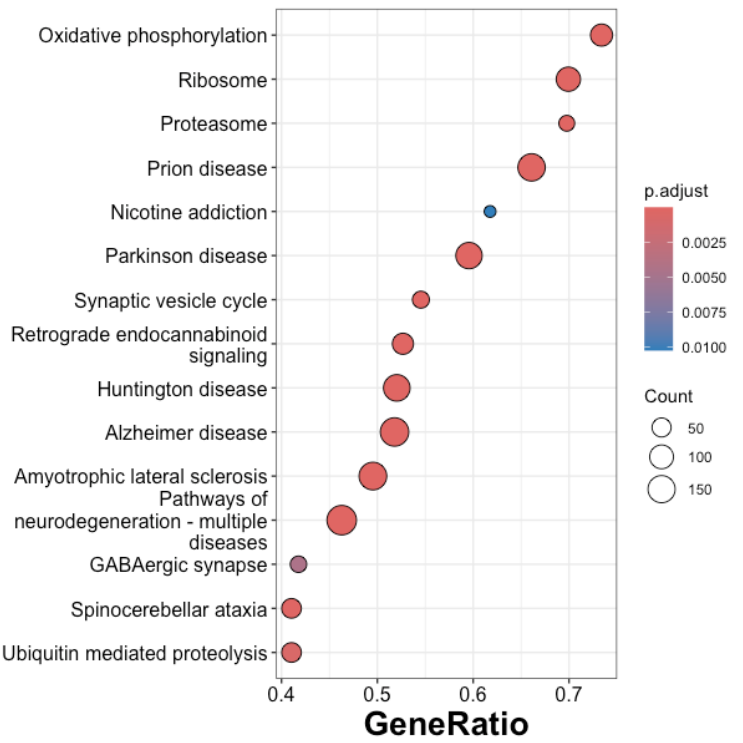

C

Overlapping GSEA terms between DART-seq and RNA-seq

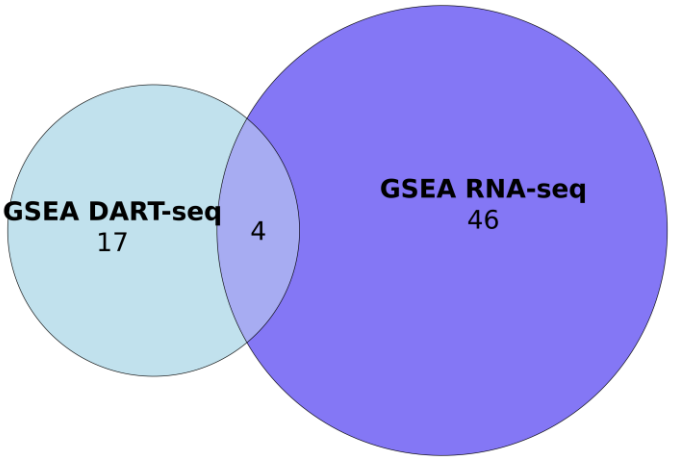

D

GABAergic synapse Log2FC

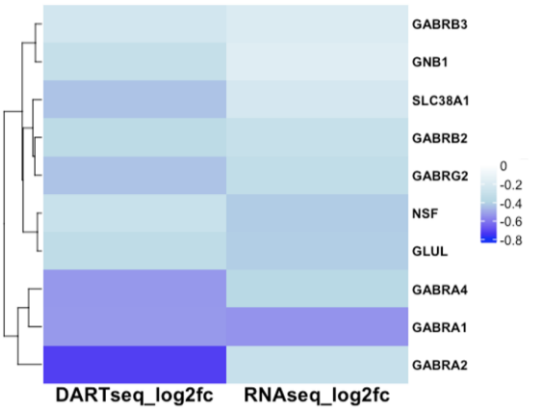

E

Nicotine addiction Log2FC

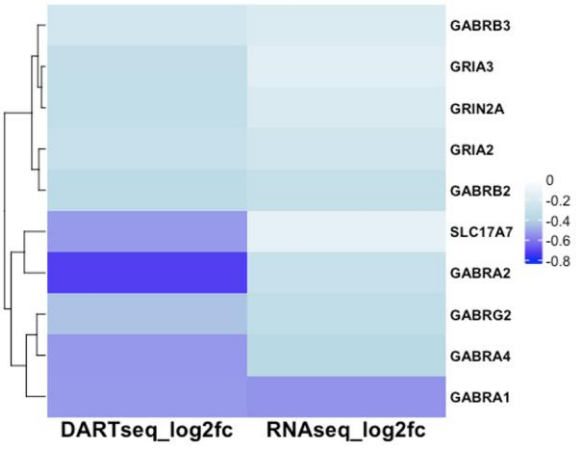

F

Synaptic vesicle cycle Log2FC

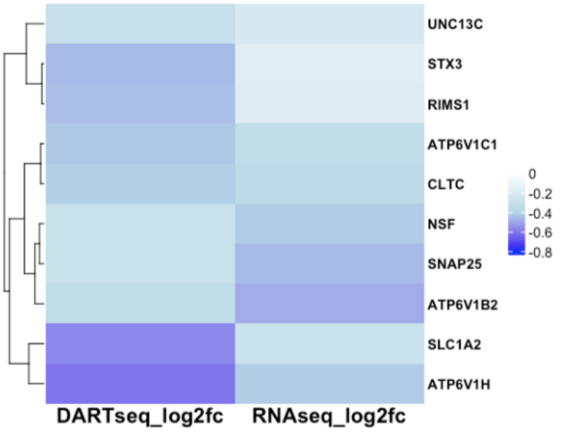

G

Ubiquitin mediated proteolysis Log2FC

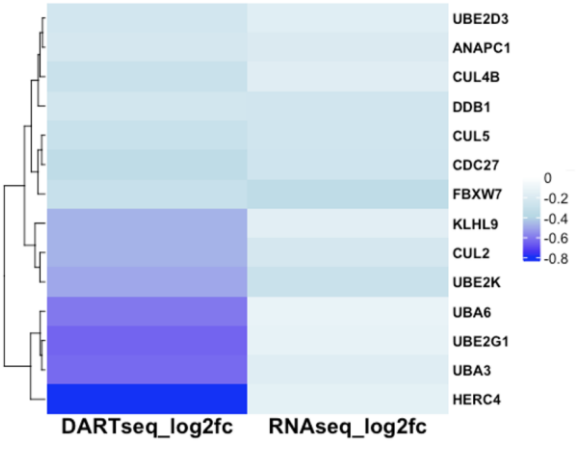

Figure 4

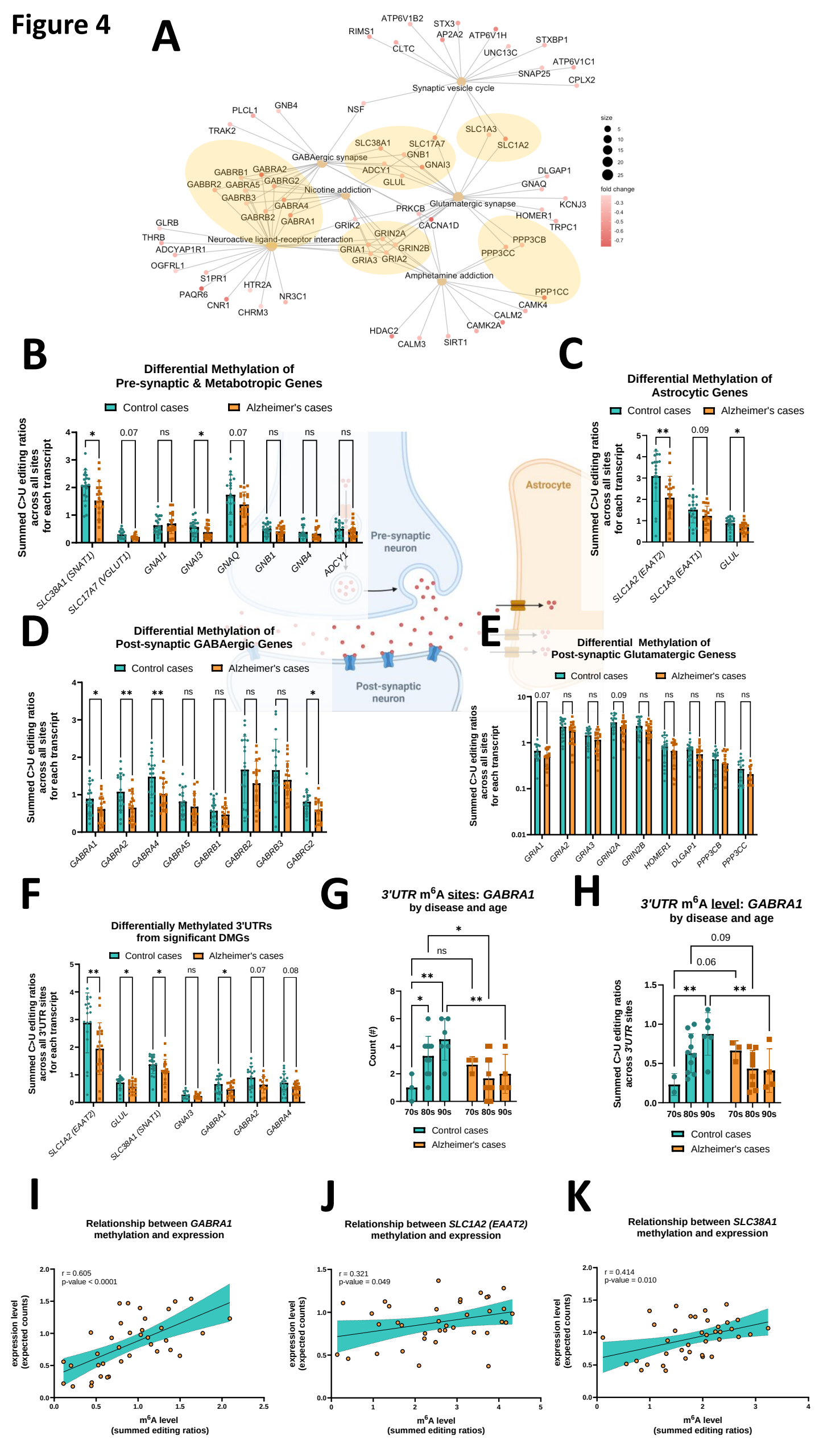
A
Synaptic vesicle cycle
GABAergic synapse
Nicotine addiction
Glutamatergic synapse
Neuroactive ligand-receptor interaction
Amphetamine addiction
size
fold change
B
Differential Methylation of Pre-synaptic & Metabotropic Genes
Control cases
Alzheimer's cases
Summed C>U editing ratios across all sites for each transcript
SLC38A1 (SNAT1)
SLC17A7 (VGLUT1)
GNAI1
GNAI3
GNAQ
GNB1
GNB4
ADCY1
Pre-synaptic neuron
Astrocyte
Post-synaptic neuron
C
Differential Methylation of Astrocytic Genes
SLC1A2 (EAAT2)
SLC1A3 (EAAT1)
GLUL
D
Differential Methylation of Post-synaptic GABAergic Genes
GABRA1
GABRA2
GABRA4
GABRA5
GABRB1
GABRB2
GABRB3
GABRG2
E
Differential Methylation of Post-synaptic Glutamatergic Geness
GRIA1
GRIA2
GRIA3
GRIN2A
GRIN2B
HOMER1
DLGAP1
PPP3CB
PPP3CC
F
Differentially Methylated 3'UTRs from significant DMGs
Summed C>U editing ratios across all 3'UTR sites for each transcript
G
3'UTR m6A sites: GABRA1 by disease and age
Count (#)
70s 80s 90s
H
3'UTR m6A level: GABRA1 by disease and age
Summed C>U editing ratios across 3'UTR sites
I
Relationship between GABRA1 methylation and expression
r = 0.605
p-value < 0.0001
expression level (expected counts)
m6A level (summed editing ratios)
J
Relationship between SLC1A2 (EAAT2) methylation and expression
r = 0.321
p-value = 0.049
K
Relationship between SLC38A1 methylation and expression
r = 0.414
p-value = 0.010

Figure 5

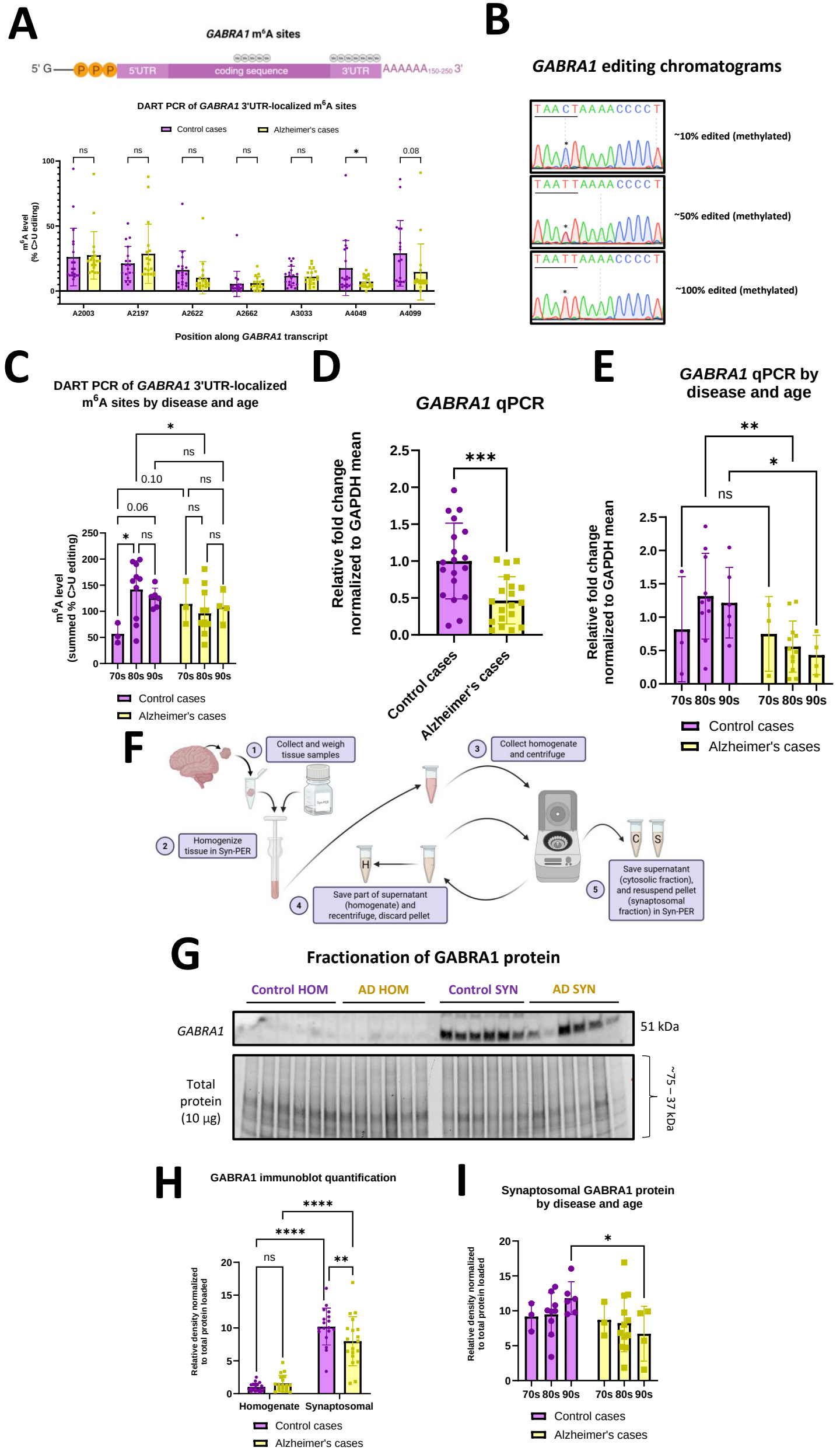
A
GABRA1 m6A sites
5' G
P P P
5'UTR
coding sequence
3'UTR
AAAAAA150-250 3'
DART PCR of GABRA1 3'UTR-localized m6A sites
Control cases
Alzheimer's cases
ns
ns
ns
ns
ns
*
0.08
m6A level (% C>U editing)
100
50
0
A2003
A2197
A2622
A2662
A3033
A4049
A4099
Position along GABRA1 transcript
B
GABRA1 editing chromatograms
TAACTAAAACCCCT
~10% edited (methylated)
TAATTAAAACCCCT
~50% edited (methylated)
TAATTAAAACCCCT
~100% edited (methylated)
C
DART PCR of GABRA1 3'UTR-localized m6A sites by disease and age
*
ns
0.10
ns
0.06
ns
*
ns
ns
m6A level (summed % C>U editing)
250
200
150
100
50
0
70s 80s 90s
70s 80s 90s
Control cases
Alzheimer's cases
D
GABRA1 qPCR
***
Relative fold change normalized to GAPDH mean
2.5
2.0
1.5
1.0
0.5
0.0
Control cases
Alzheimer's cases
E
GABRA1 qPCR by disease and age
**
*
ns
Relative fold change normalized to GAPDH mean
2.5
2.0
1.5
1.0
0.5
0.0
70s 80s 90s
70s 80s 90s
Control cases
Alzheimer's cases
F
1 Collect and weigh tissue samples
2 Homogenize tissue in Syn-PER
3 Collect homogenate and centrifuge
4 Save part of supernatant (homogenate) and recentrifuge, discard pellet
5 Save supernatant (cytosolic fraction), and resuspend pellet (synaptosomal fraction) in Syn-PER
H
C
S
G
Fractionation of GABRA1 protein
Control HOM
AD HOM
Control SYN
AD SYN
GABRA1
51 kDa
Total protein (10 µg)
~75 – 37 kDa
H
GABRA1 immunoblot quantification
****
****
ns
**
Relative density normalized to total protein loaded
20
15
10
5
0
Homogenate
Synaptosomal
Control cases
Alzheimer's cases
I
Synaptosomal GABRA1 protein by disease and age
*
Relative density normalized to total protein loaded
20
15
10
5
0
70s 80s 90s
70s 80s 90s
Control cases
Alzheimer's cases

Figure 6

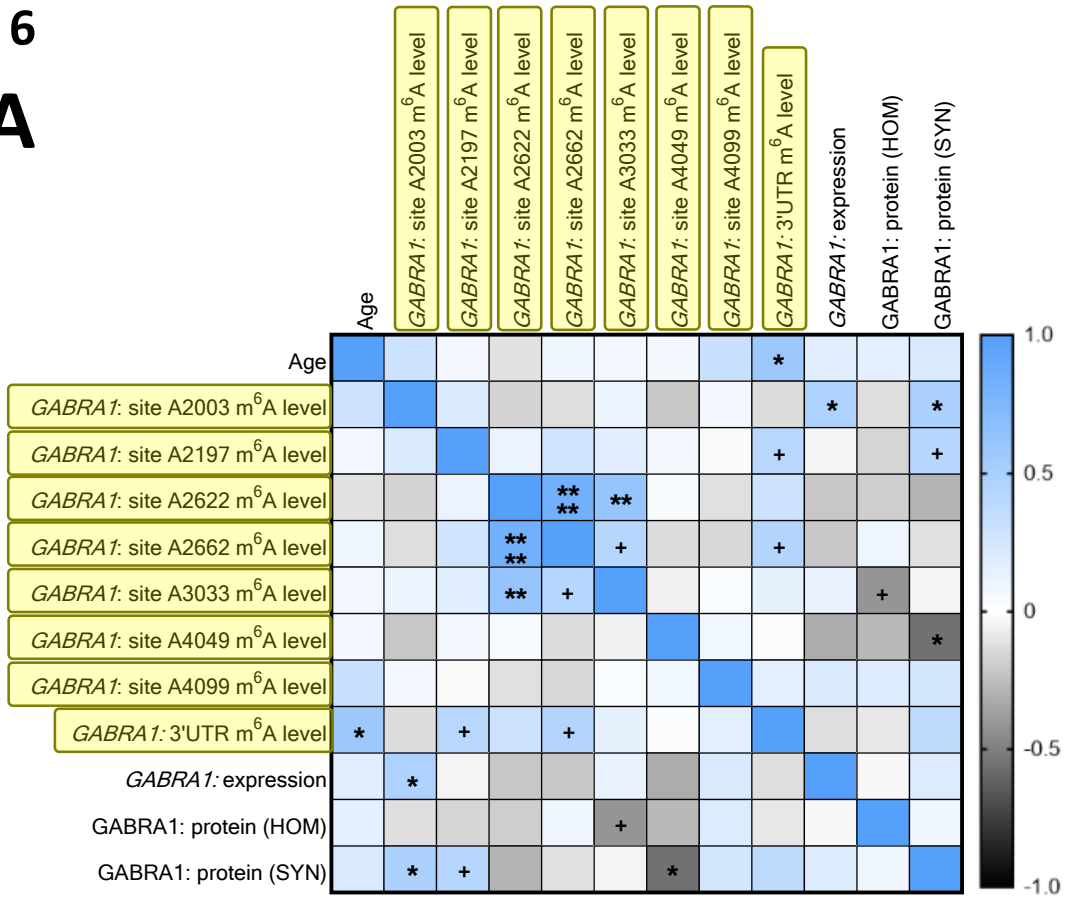
A
Age
GABRA1: site A2003 m6A level
GABRA1: site A2197 m6A level
GABRA1: site A2622 m6A level
GABRA1: site A2662 m6A level
GABRA1: site A3033 m6A level
GABRA1: site A4049 m6A level
GABRA1: site A4099 m6A level
GABRA1: 3'UTR m6A level
GABRA1: expression
GABRA1: protein (HOM)
GABRA1: protein (SYN)
1.0
0.5
0
-0.5
-1.0

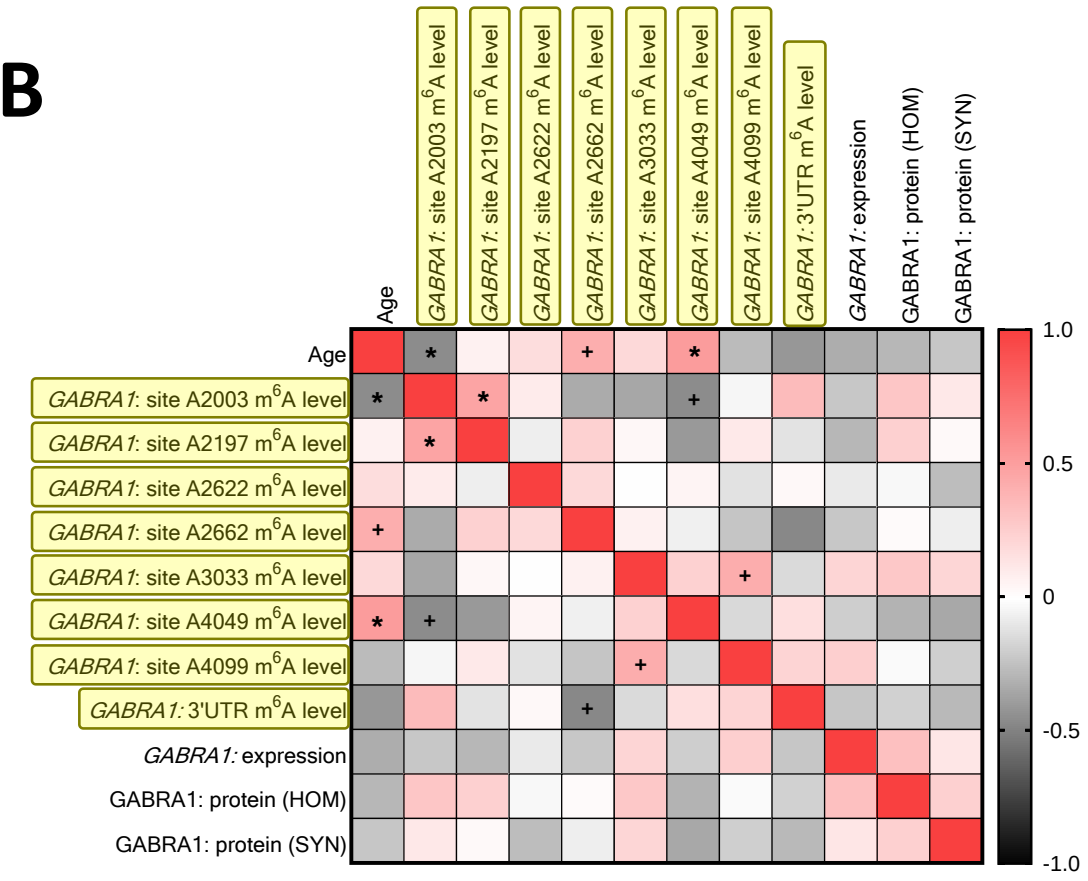
B
Age
GABRA1: site A2003 m6A level
GABRA1: site A2197 m6A level
GABRA1: site A2622 m6A level
GABRA1: site A2662 m6A level
GABRA1: site A3033 m6A level
GABRA1: site A4049 m6A level
GABRA1: site A4099 m6A level
GABRA1: 3'UTR m6A level
GABRA1: expression
GABRA1: protein (HOM)
GABRA1: protein (SYN)
1.0
0.5
0
-0.5
-1.0

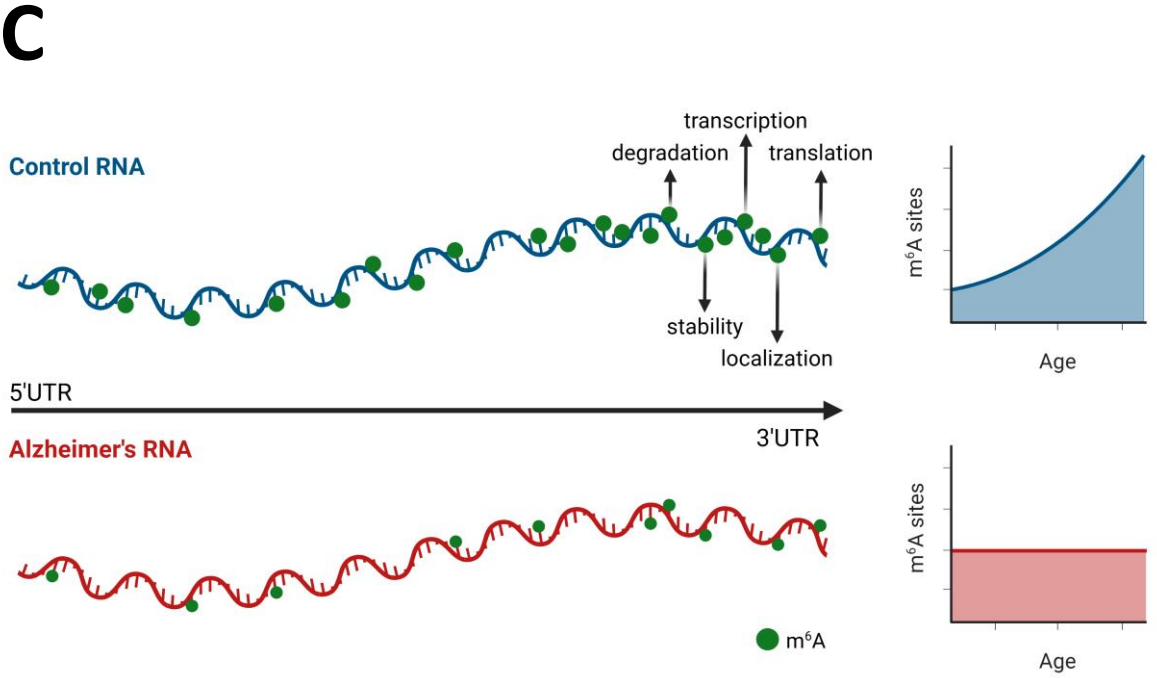
C
Control RNA
transcription
degradation
translation
stability
localization
5'UTR
3'UTR
m6A sites
Age
Alzheimer's RNA
m6A
m6A sites
Age

Supplemental Figure 1

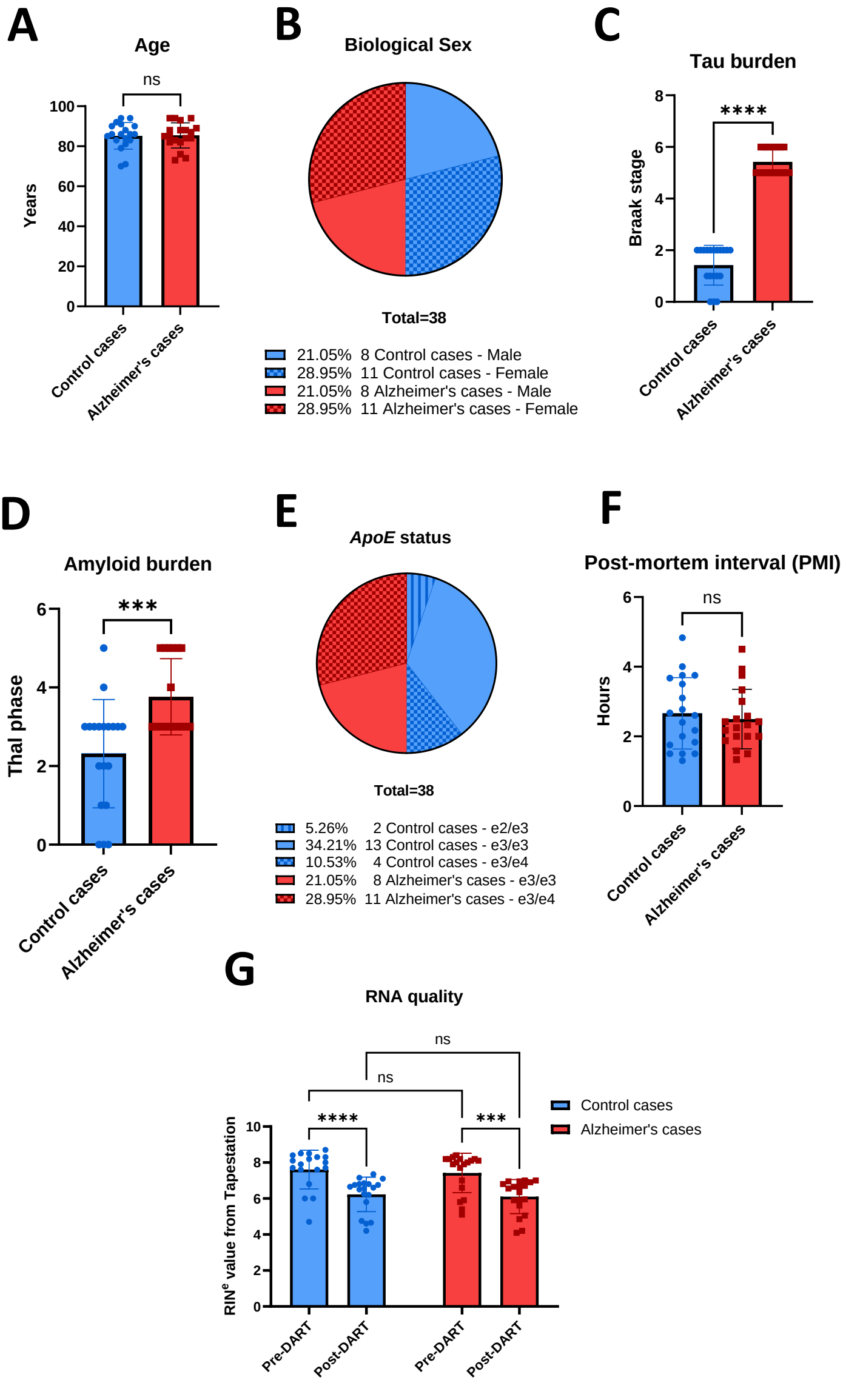

Supplemental Figure 2

A

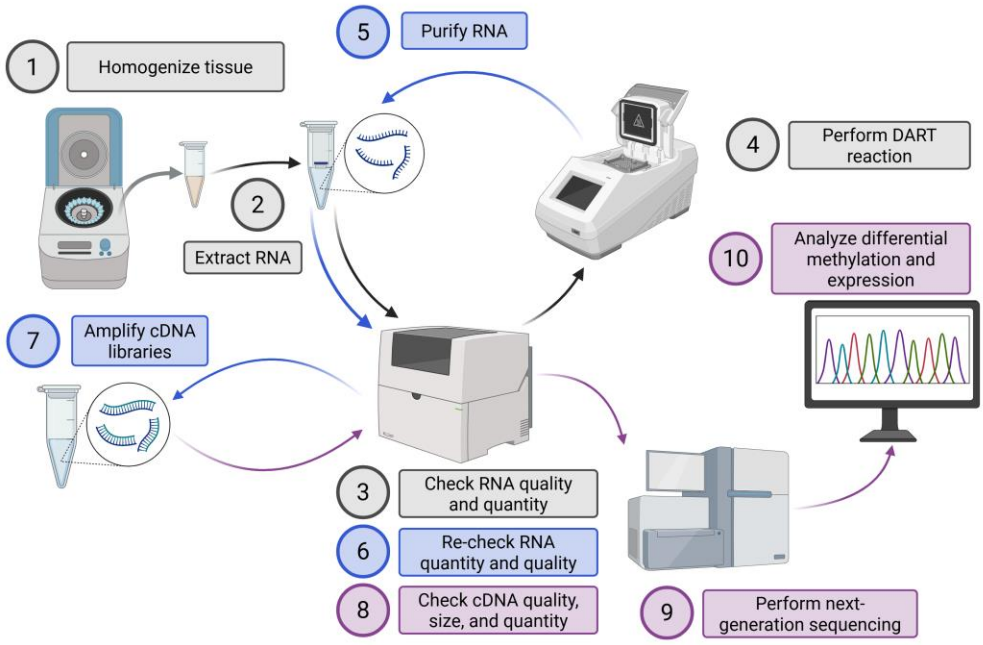

B

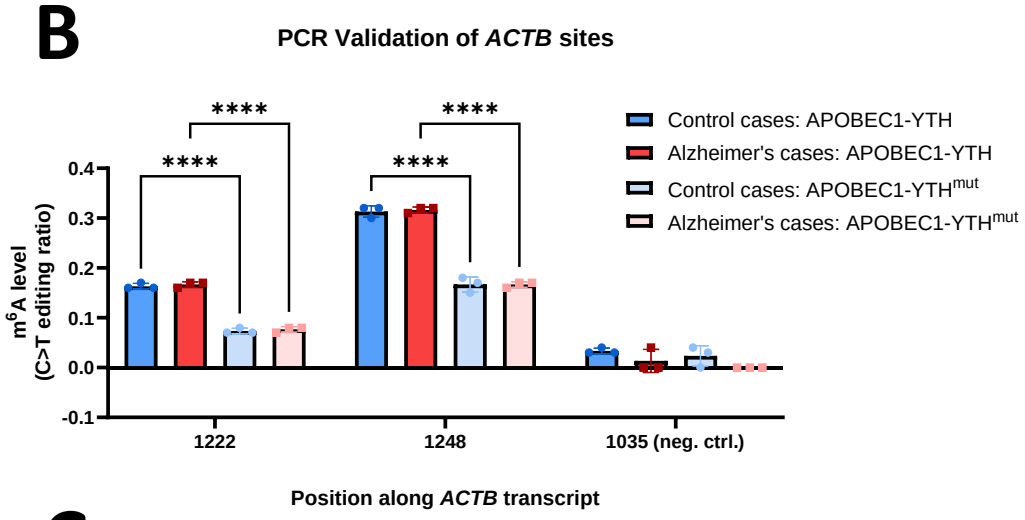

C

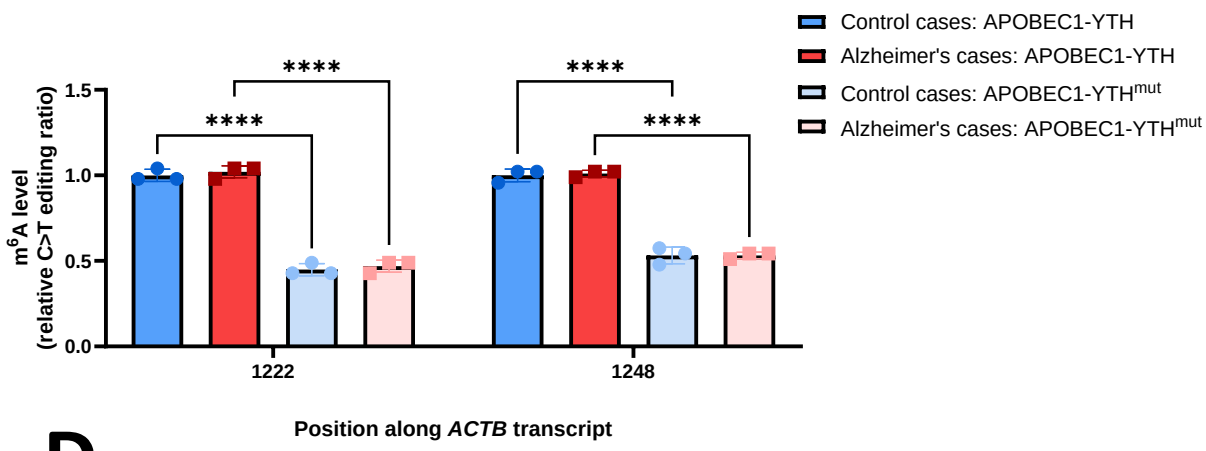

D

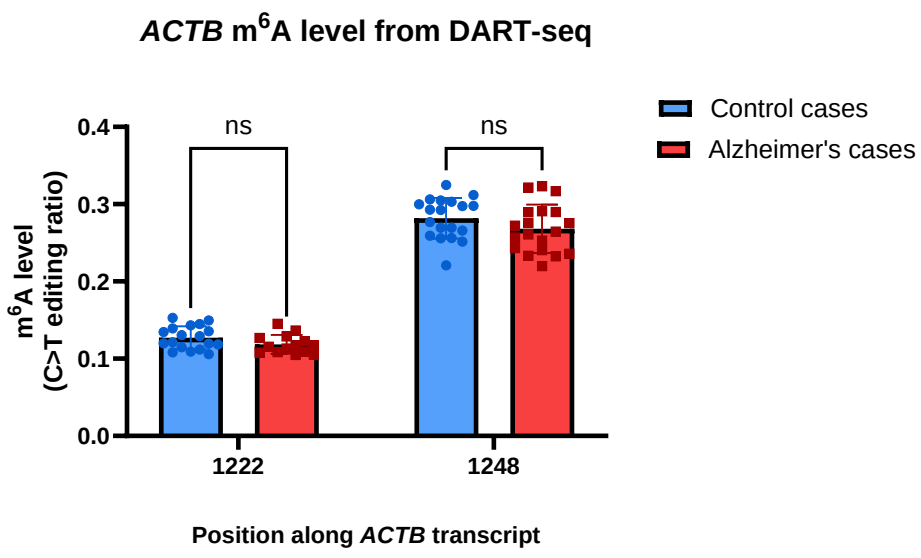

Supplemental Figure 3

A

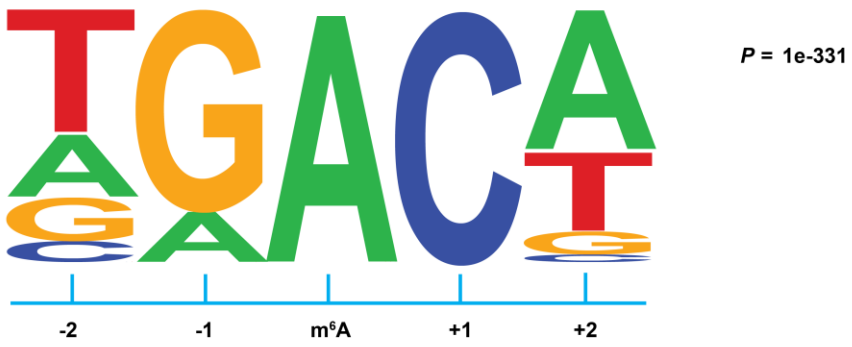

B

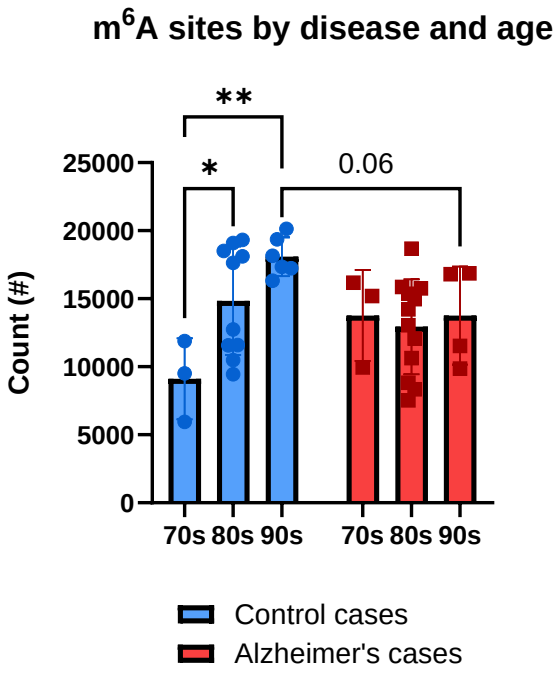

Supplemental Figure 4

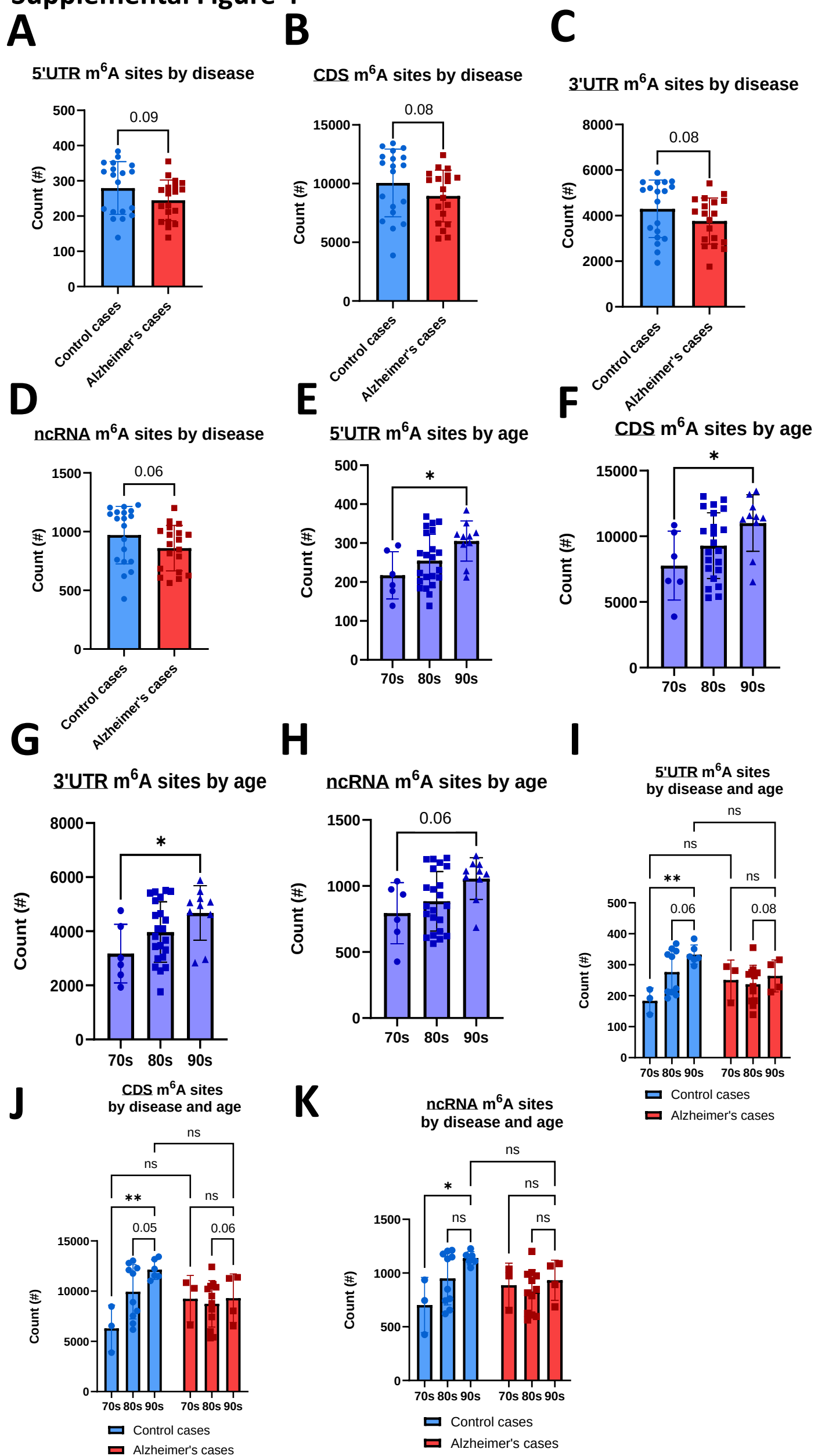

Supplemental Figure 5

A

GO CC analysis of genes with m^{6}A sites

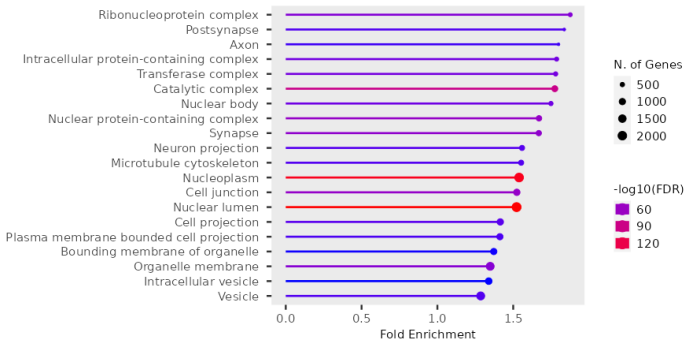

B

GO CC analysis of genes with 5'UTR m^{6}A sites (using all genes with m^{6}A sites as background)

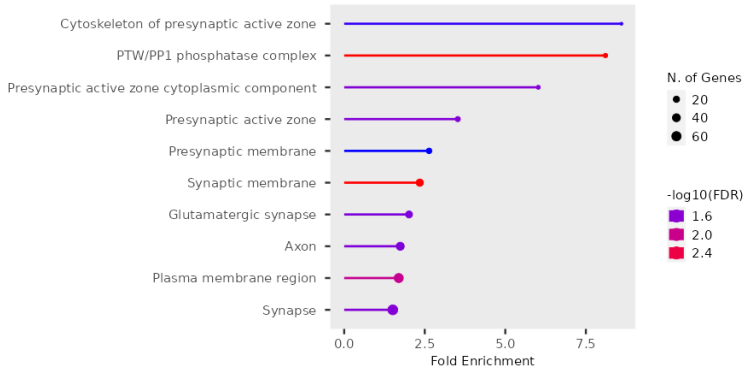

C

GO CC analysis of genes with CDS m^{6}A sites (using all genes with m^{6}A sites as background)

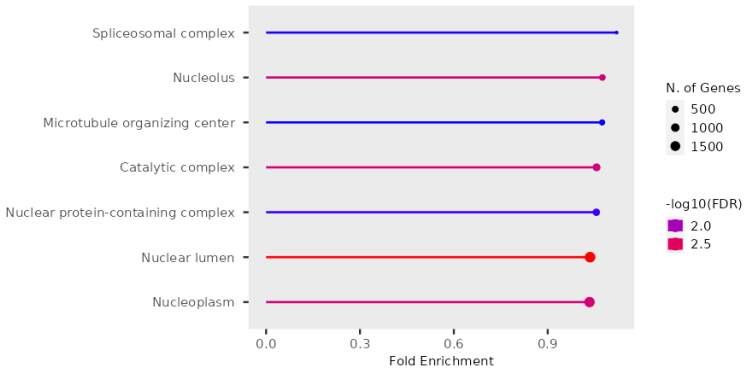

D

GO CC analysis of genes with 3'UTR m^{6}A sites (using all genes with m^{6}A sites as background)

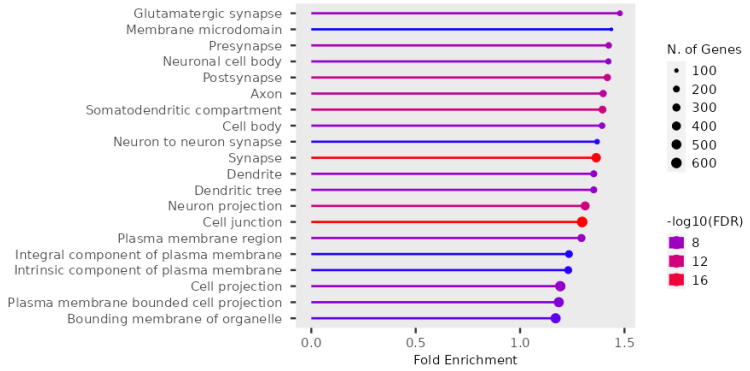

E

GO CC analysis of ncRNA with m^{6}A sites (using all genes with m^{6}A sites as background)

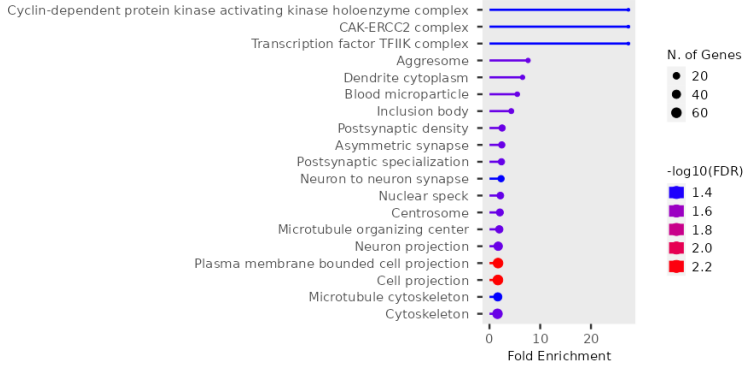

Supplemental Figure 6

A

Differentially abundant sites: Control cases

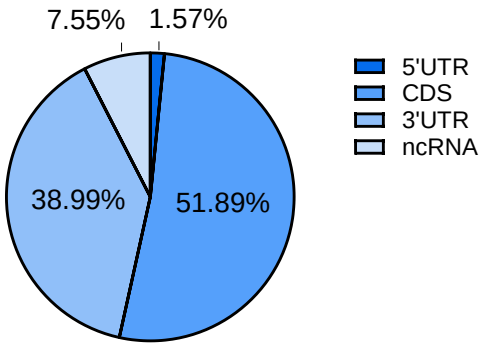

Sites: 328
Genes: 209

B

Differentially abundant sites: AD cases

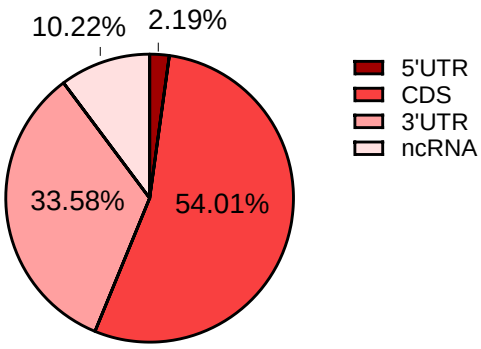

Sites: 137
Genes: 131

C

Relative frequency of differentially abundant sites by domain

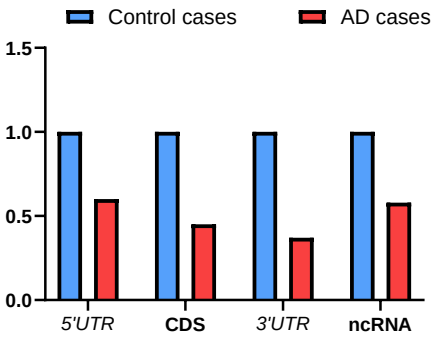

D

m^{6}A level of select (DAS)

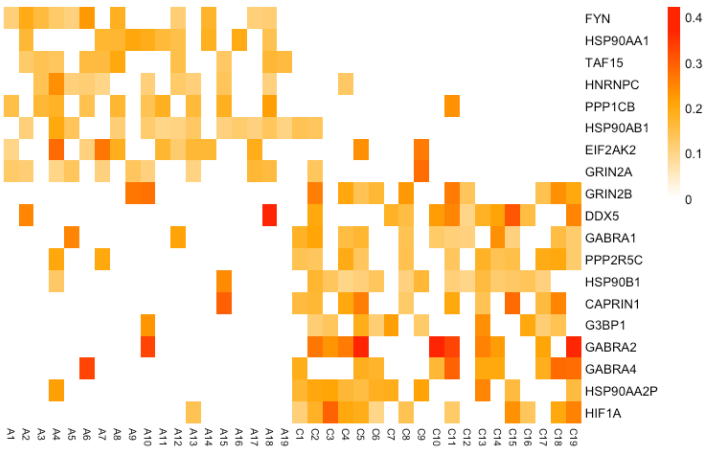

E

m^{6}A level of unique (DAS)

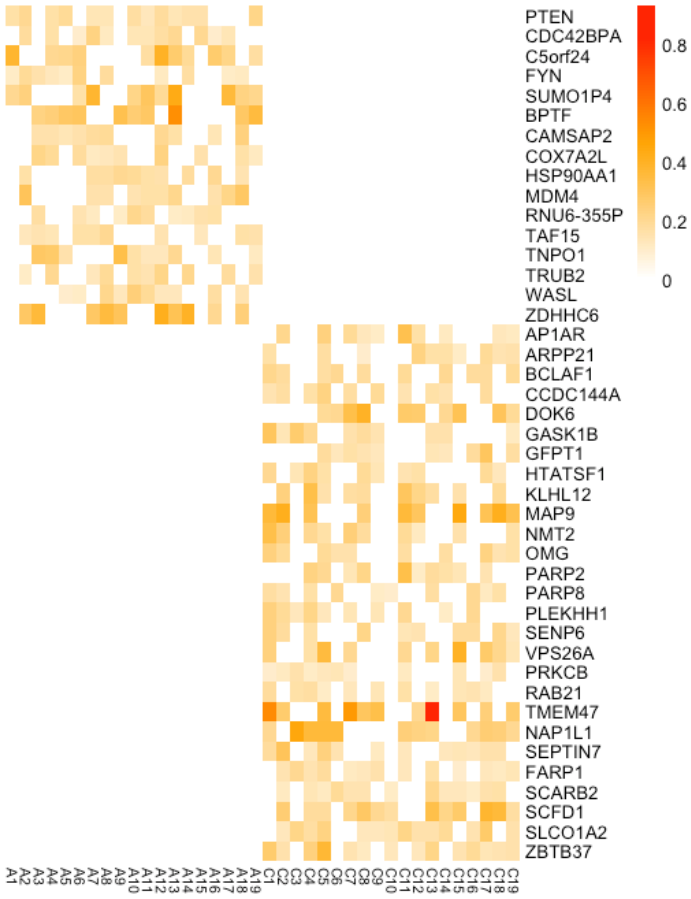

F

GO MF of genes with DAS (Control)

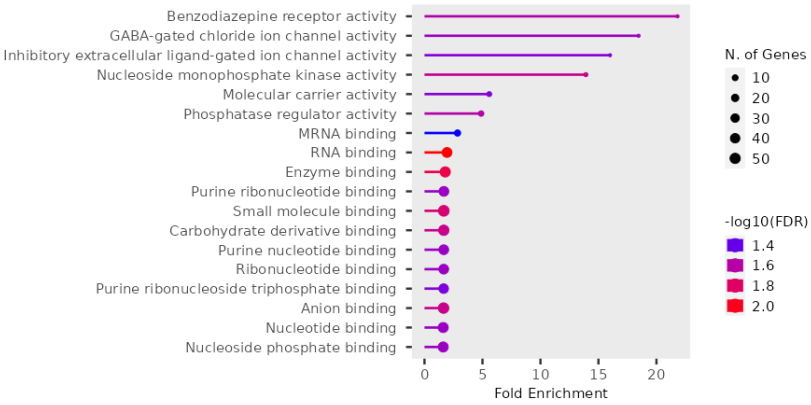

G

GO CC of genes with DAS (AD)

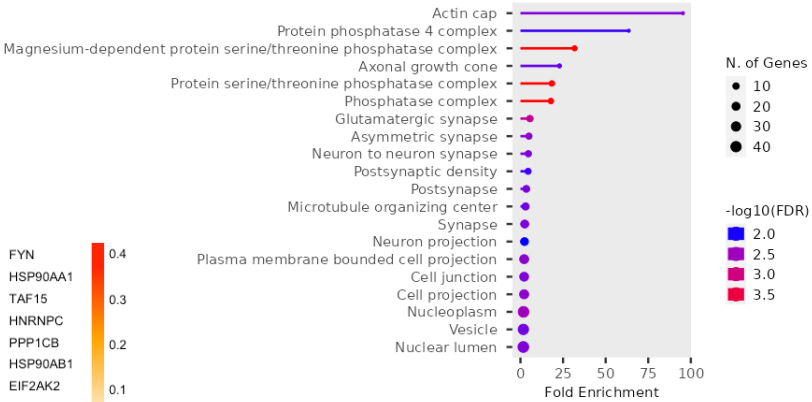

Supplemental Figure 7

A

Overlapping DEGs and differentially methylated 5'UTR

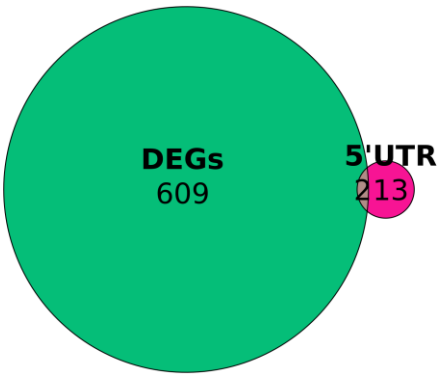

B

DEGs with differentially methylated 5'UTR

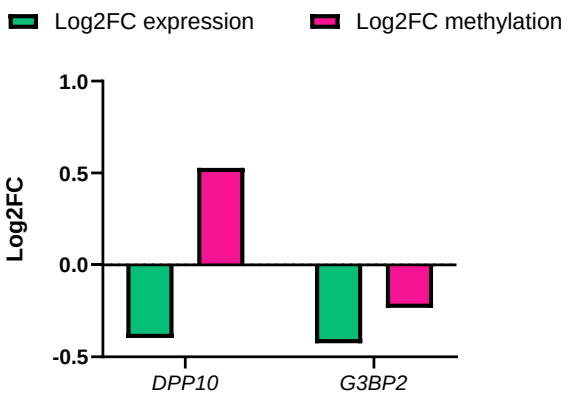

C

Overlapping DEGs and differentially methylated CDS

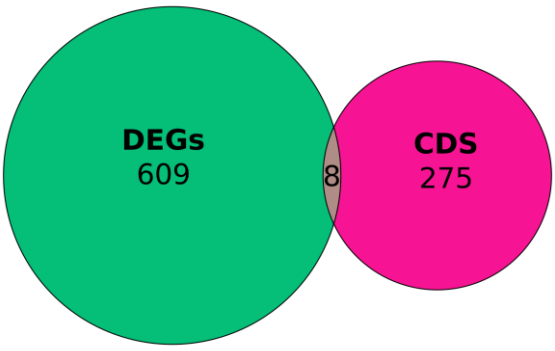

D

DEGs with differentially methylated CDS

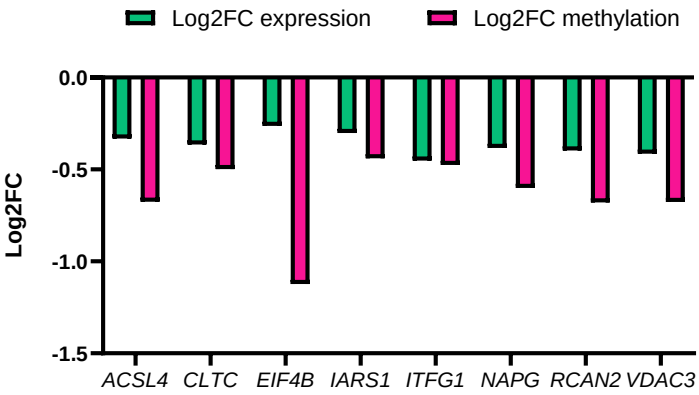

E

Overlapping DEGs and differentially methylated 3'UTR

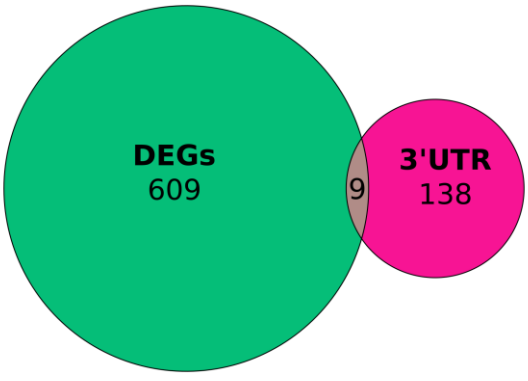

F

DEGs with differentially methylated 3'UTR

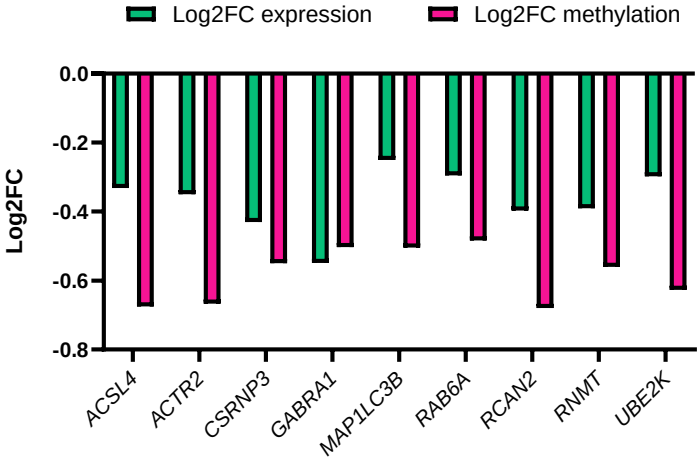

G

Overlapping DEGs and differentially methylated ncRNA

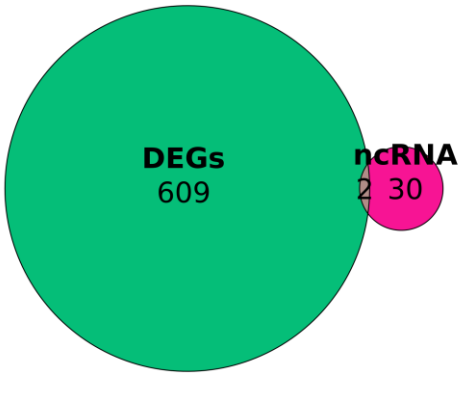

H

DEGs with differentially methylated ncRNA

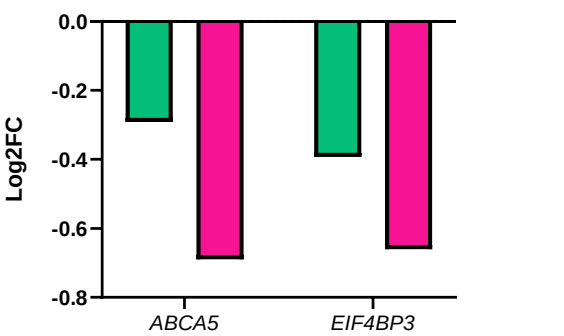

Supplemental Figure 8

A — *GABRA2*

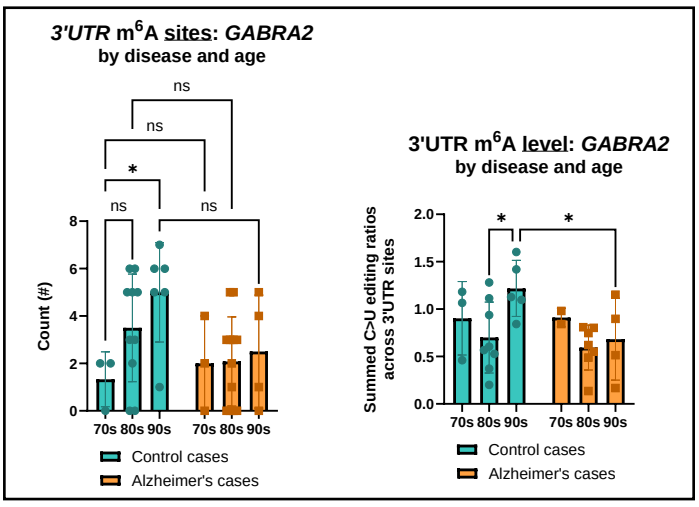

B — *GABRA4*

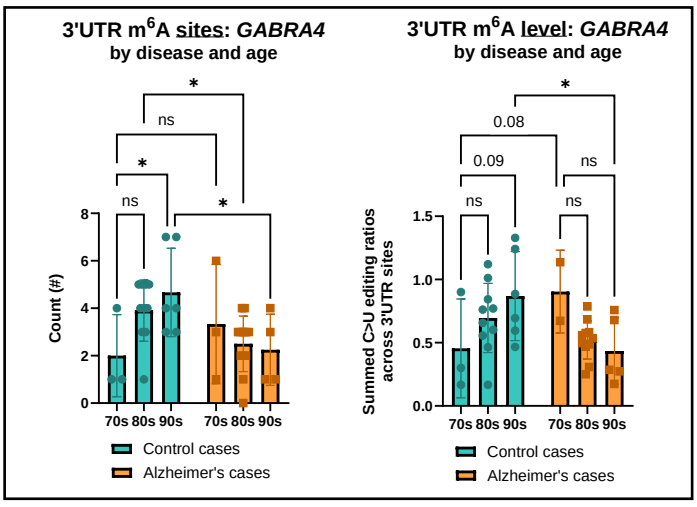

C — *SLC38A1*

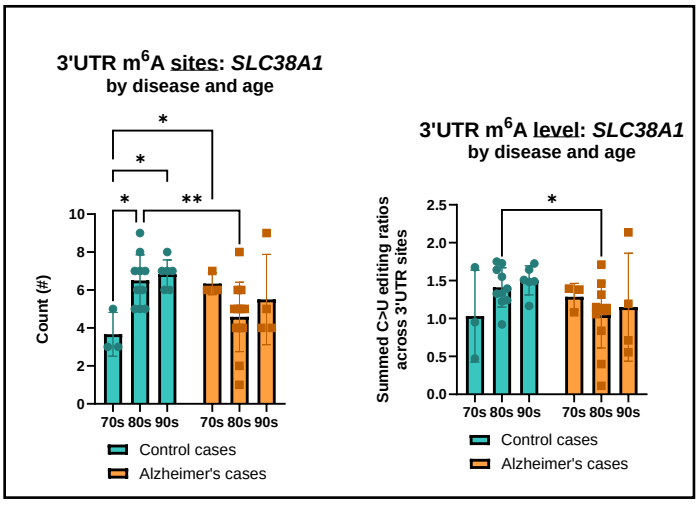

D — *GNAI3*

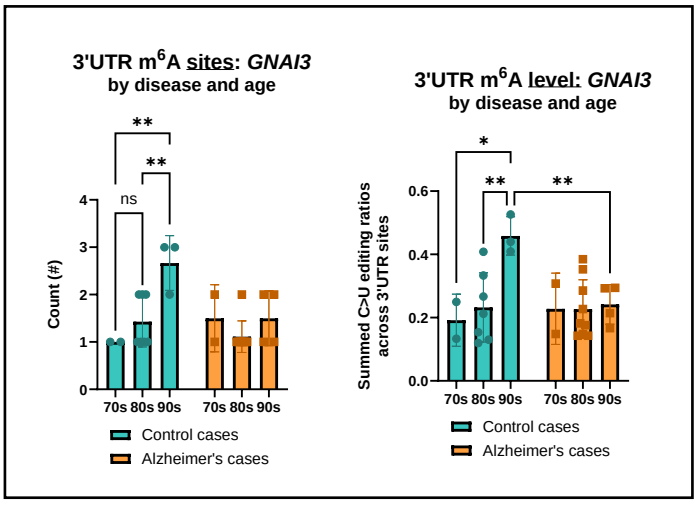

E — *SLC1A2*

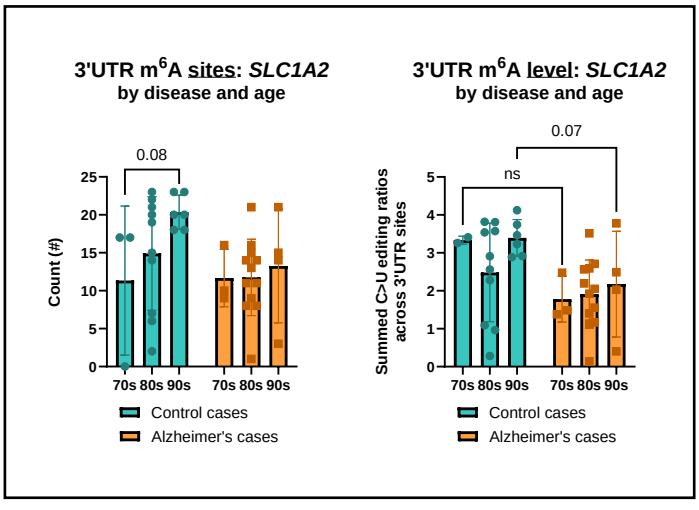

F — *GLUL*

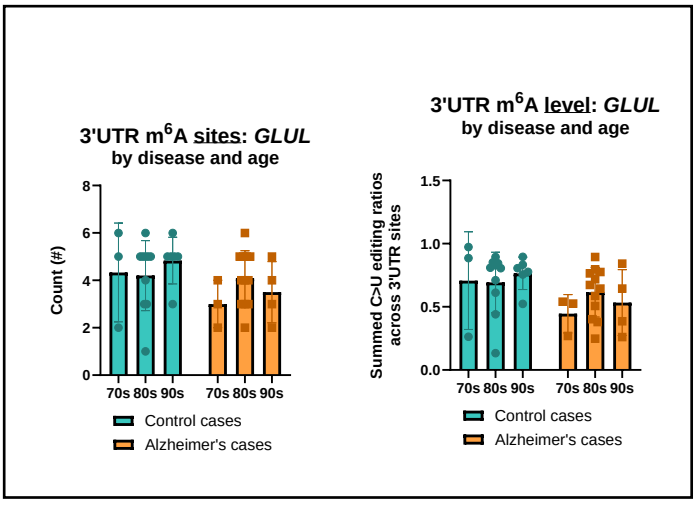
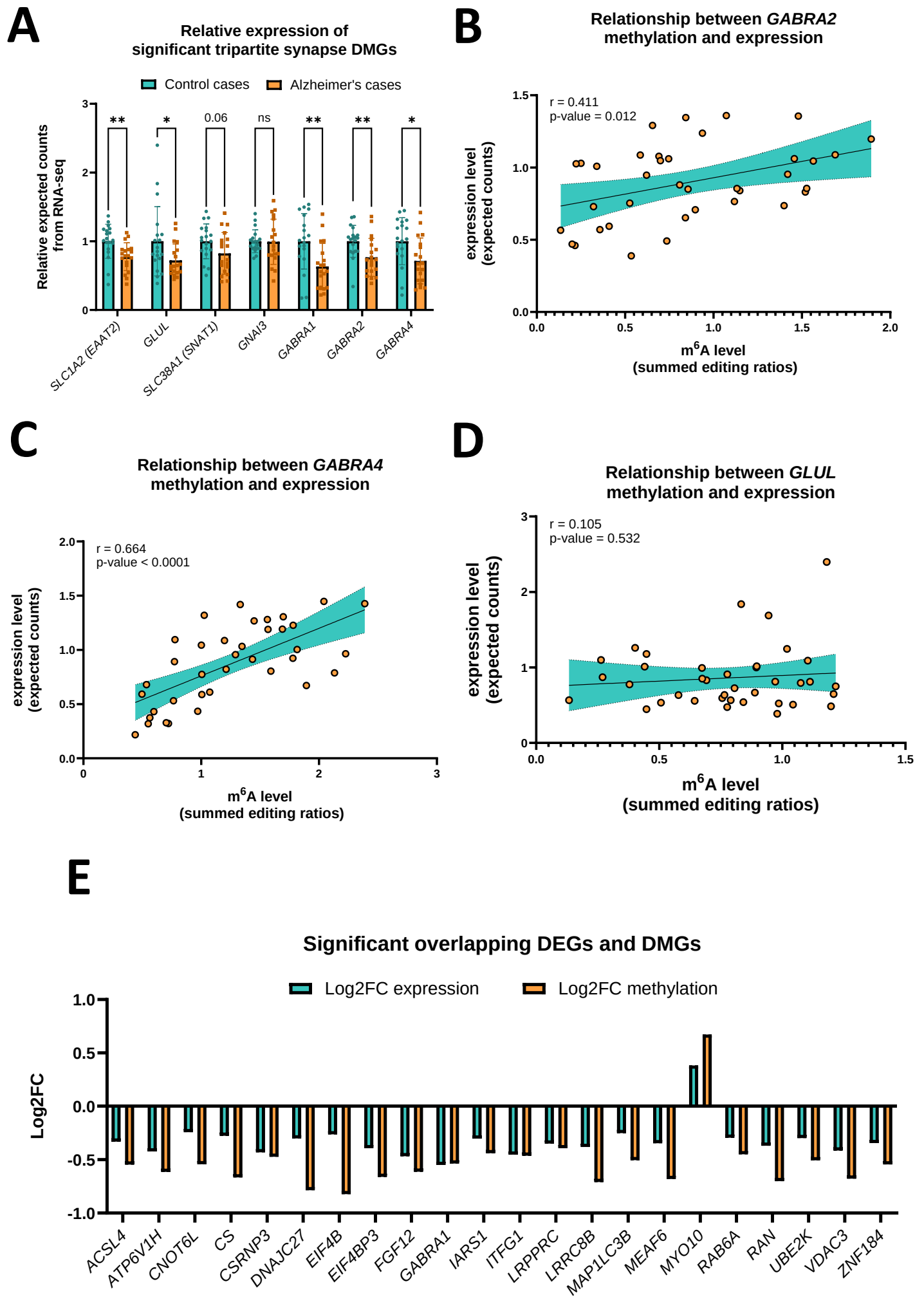
Supplemental Figure 9